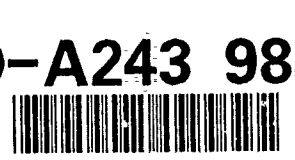

(2)

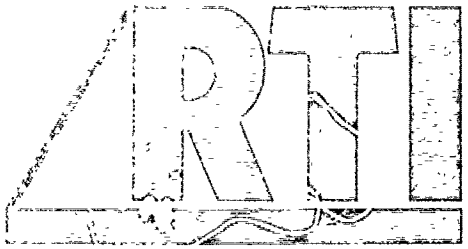

RESEARCH TRIANGLE INSTITUTE

RTI/3629/91-Quarterly

December 1991

SEMICONDUCTOR DIAMOND TECHNOLOGY

Quarterly Report -- Second Quarter
1 April 1991 - 30 June 1991

R. J. Markunas
R. A. Rudder
J. B. Posthill
R. E. Thomas

STRATEGIC DEFENSE INITIATIVE ORGANIZATION
Innovative Science and Technology Office

Office of Naval Research
Program No.
N00014-86-C-0460

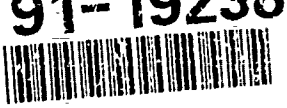

POST OFFICE BOX 12194 RESEARCH TRIANGLE PARK, NORTH CAROLINA 27709-2194

REPORT DOCUMENTATION PAGE

Form Approved
OMB No 0704-0188

1. AGENCY USE ONLY *(Leave blank)*	2. REPORT DATE	3. REPORT TYPE AND DATES COVERED
		Quarterly Report, 1 April 1991-30 June 1991

4. TITLE AND SUBTITLE

Semiconductor Diamond Technology

5. FUNDING NUMBERS

N00014-86-C-0460

6. AUTHOR(S)

R.J. Markunas, R.A. Rudder, J.B. Posthill, R.E. Thomas

7. PERFORMING ORGANIZATION NAME(S) AND ADDRESS(ES)

Research Triangle Institute
P.O. Box 12194
Research Triangle Park, NC 27709

8. PERFORMING ORGANIZATION REPORT NUMBER

83U-3629

9. SPONSORING/MONITORING AGENCY NAME(S) AND ADDRESS(ES)

Office of Naval Research
800 N. Quincy Street
Arlington, VA 22217-5000

10. SPONSORING/MONITORING AGENCY REPORT NUMBER

11. SUPPLEMENTARY NOTES

12a. DISTRIBUTION/AVAILABILITY STATEMENT

Approved for public release; unlimited distribution

12b. DISTRIBUTION CODE

13. ABSTRACT *(Maximum 200 words)*

Workers at Research Triangle Institute presented 5 papers to the Electrochemical Society meeting in Washington. These papers represent work in 1) surface chemistry, 2) gas-phase diagnostics, 3) homoepitaxial growth, 4) IGFET fabrication, and 5) halogen-assisted CVD. Of particular interest was the excellent surface chemistry work presented by Dr. Raymond Thomas expounding the roles of atomic hydrogen on the diamond (100) surface. Atomic hydrogen chemisorbs on the diamond surface at monolayer saturations. Atomic hydrogen does not readily insert on the carbon surface dimer bonds. At dose levels exceeding a monolayer, CH_3 and C_2H_2 desorptions are detected at temperatures $\sim 200\,^{\circ}C$ colder than the H desorption.

In addition, preliminary work this quarter showed the capability to produce diamond films from a water-based process which does not involve molecular hydrogen as a process gas. Subsequent quarterly reports will give more details on this process.

14. SUBJECT TERMS

15. NUMBER OF PAGES

56

16. PRICE CODE

17. SECURITY CLASSIFICATION OF REPORT	18. SECURITY CLASSIFICATION OF THIS PAGE	19. SECURITY CLASSIFICATION OF ABSTRACT	20. LIMITATION OF ABSTRACT
unclassified	unclassified	unclassified	

TABLE OF CONTENTS

1.0 SUMMARY OF PROGRESS

This is the 1991 Second Quarterly Report on the Semiconducting Diamond Program Contract No. N-00014-C-0138 at Research Triangle Institute. Work on the diamond program during this quarter mainly centered around preparing for the Electrochemical Society Meeting in May. Research Triangle Institute participated in that meeting by delivering 5 oral presentations along with submission of the corresponding papers for publication in the conference proceedings. In addition, collaborative work with Kobe Research lead to a sixth presentation and publication. The associated papers for all those presentations are included in this quarterly report. Details are found within. Results from those papers showed the breadth and depth of the diamond research activities at Research Triangle Institute. The papers included results on diamond synthesis (plasma-based and thermal-based processes), FET fabrication and evaluation, natural diamond substrate evaluation (problems to be addressed for homoeptiaxial growth), surface chemistry, and Schottky barrier formation using thin SiO_2 remote plasma oxides.

Of these papers, the surface chemistry work generated the most excitement at the conference. Dr. Raymond Thomas presented results for thermal desorption from hydrogenated diamond (100) surfaces. The small sample size makes delineation of the hydrogen desorption spectrum from hydrogen background in the reactor extremely difficult. Improvements in heater design (molybdenum fixturing, laser drilled holes in the diamond for wiring the sample to the molybdenum heater stage, imbedment of the thermocouple in the diamond for accurate temperature measurement) and nearly complete

vacuum isolation of the quadrupole chamber from the sample chamber permitted accurate recording of the hydrogen desorption spectrum. The results were different from those reported previously by other workers, and the desorption results from diamond were very different from hydrogen on Si(100) surfaces. The results showed saturation of the (100) surfaces with hydrogen at near monolayer coverages. The surfaces did not adsorb additional hydrogen. Atomic hydrogen did not readily insert on the 2×1 diamond surface dimers. Correspondingly, exceedingly high doses of atomic hydrogen (comparable to the dose that a CVD diamond film might experience) was necessary to convert the 2×1 surface state to a 1×1 bulk-like structure. Given the observed methyl and acetylenic desorptions from the surface, it is reasonable to expect that the surface dimer units may have desorbed from the surface rather than hydrogen inserting on the dimer bond site. Work is continuing in the surface chemistry facility. In particular the role of oxygen on the diamond (100) surface is being evaluated. The interest in the role of oxygen on diamond growth has been heightened by work this quarter at RTI for the growth of diamond films using water-alcohol mixtures with no molecular hydrogen addition to the plasma.

A novel, low temperature growth technique for the chemical vapor deposition (CVD) of diamond films from low-pressure rf-plasma discharges containing principally water vapor has been discovered. Carbon for diamond deposition was supplied to the plasma gas by admitting alcohol vapor with the water vapor. No other gasses were admitted to the growth chamber. Hence, this work is quite different from the work of Saito et al.[16,17] wherein 0- 6% concentrations of water in H_2 - CH_4 microwave plasmas

were investigated for diamond growth. In this work, the predominantly water-based discharges produce OH and H radicals. The water discharge becomes the functionally equivalent to a molecular hydrogen discharges in other diamond CVD techniques. Emission from a pure water discharge and the water-alcohol discharges show strong H_α emission and OH emission. The atomic hydrogen emission from a pure water rf-plasma discharge at 1.0 Torr is so dominant that the plasma has a characteristic red color from the 656 nm emission. The ratio of water to alcohol admitted to the growth chamber was fixed by the partial pressures of water and alcohol above the mixed solutions of 20% alcohol in water. The morphology of the polycrystalline films was dependent on the choice of alcohol. Distinct differences were observed both in nucleation density and crystalline morphology. In addition to polycrystalline growth, homoepitaxial diamond growth has been accomplished.

More results from this process will be disclosed during subsequent quarterly reports.

APPENDIX

THERMAL DESORPTION FROM HYDROGENATED DIAMOND (100) SURFACES

R.E. Thomas, R.A. Rudder, R.J. Markunas
Research Triangle Institute, Research Triangle Park, NC 27709

ABSTRACT

Thermal desorption spectroscopy and low energy electron diffraction (LEED) have been used to study the interaction of atomic hydrogen with the diamond (100) surface. Heating a diamond crystal in-vacua readily reconstructs the surface from a (1x1) configuration to a (2x1) structure. Unlike the case for silicon, exposure to atomic hydrogen does not easily convert the surface back to the (1x1) structure. Hydrogen thermal desorption peaks from the (2x1) surface exposed to atomic hydrogen at $1x10^{-6}$ Torr are seen at approximately 950 °C for heating rates of 20 °C/sec. After exposure of the surface to atomic hydrogen in amounts in excess of that required to terminate the surface, 10^{-2} Torr, thermal desorption peaks associated with methyl radicals and acetylene are observed in addition to hydrogen. Upon further exposure at 10 Torr the surface appears to be partially converted to a (1x1) structure and acetylene desorption features are no longer observed.

Introduction

Hydrogen plays a key role in most diamond growth processes developed to date. However, the details of the behavior of hydrogen on the diamond surface are not well understood. It is thought to both etch non—sp^3 bonded carbon, which may be deposited during the growth process, and to stabilize the cubic structure on the growing diamond surface by terminating dangling bonds. Previous studies of hydrogen interactions on diamond indicate that hydrogen desorbs from the surface at approximately 900 °C (1,2). Typically, researchers find that heating the diamond to approximately 1000 °C results in the (1x1) surface structure converting to the (2x1) surface structure (2,3). One might expect, as in the case of silicon, the surface would convert back to the (1x1) state upon exposure to atomic hydrogen. Hamza et al. have observed the transition back to a (1x1) configuration on exposure to atomic hydrogen but find that on subsequent annealing the (2x1) surface is not recovered (2).

In the present work thermal desorption spectroscopy and LEED were used to study interactions of atomic hydrogen with the diamond (100) surface. Transitions from the (1x1) phase to (2x1) phase upon annealing and from the (2x1) phase to the (1x1) phase upon exposure to atomic hydrogen were studied with LEED. Thermal desorption spectroscopy was used to determine desorption kinetics and products from hydrogen terminated surfaces.

Experimental

Thermal desorption spectroscopy and LEED observations were performed in a stainless steel UHV system. Base pressure was $5x10^{-10}$ Torr for the sample chamber and $1x10^{-10}$ Torr for the quadrupole chamber. The sample chamber was separated from the quadrupole chamber by a 2mm diameter aperture. Sample heating was accomplished by clipping the crystals to a 0.25mm thick molybdenum resistive strip heater. All parts associated with the heater stage, including the clamps and current leads were manufactured from molybdenum. The sample temperature was measured by a 0.125mm diameter chromel/alumel thermocouple in intimate contact with the crystal. The thermocouple was threaded through a hole in one corner of the crystal, and the thermocouple bead then held in tension against the crystal. Two (100), 5mmx5mmx0.25mm, diamond crystals were used in the course of the present study. One of the crystals had approximately .5 microns of homoepitaxial diamond deposited prior to insertion into the system. Diamond polishing of the substrates leaves fine scratch marks on the surface, which previous work has shown can be covered by deposition of a homoepitaxial film (4). The homoepitaxial diamond was grown with an rf discharge plasma CVD process using CH_4 in H_2 as feedstock. The uncoated samples were cleaned by hand-polishing with 0.25 micron diamond grit and water. Following the polishing, the samples were ultrasonically cleaned in two series of baths of TCE, acetone, and methanol. Between solvent bath series the samples were vigorously swabbed to remove particulates. Once the samples were introduced to the chamber, no additional cleaning was performed aside from thermal desorption of adsorbed species. Several pressure regimes were used in dosing with atomic hydrogen, which necessitated slightly different procedures. For samples dosed at pressures from $1x10^{-7}$ Torr to $1x10^{-5}$ Torr, the hydrogen was flowing through the system. Samples were also dosed at pressures of 10^{-3} Torr-10^{-2} Torr and 1-10 Torr. For these samples the main chamber was sealed and hydrogen was admitted to the desired pressure. In all cases atomic hydrogen was generated via a tungsten filament operating at a temperature of approximately 1500 °C. The sample was positioned approximately 2 cm. from the filament during dosing. The sample was not actively cooled and at the lowest dosing pressures remained at room temperature. At dosing pressures in the 1-10 Torr range the sample temperature rose to approximately 125 °C. All thermal desorption spectra were taken with a heating rate of 20 °C/sec.

Results

The surface structure of the samples was monitored with LEED immediately after introduction to the chamber, after dosing, and after thermal desorptions. All samples exhibited a LEED pattern without annealing. For most samples this was a (1x1) configuration. The one exception was the homoepitaxial sample which gave a (2x1) pattern. Since this sample remained at the growth temperature, 800-900 °C, while the plasma and the gasses were shut off, it is likely that surface hydrogen simply desorbed and consequently the surface reconstructed before the sample was removed from the growth chamber. Upon annealing to 800 °C-1000 °C and for times ranging from 5 seconds to 120 seconds, all samples exhibited some degree of reconstruction to the (2x1) configuration. Annealing at temperatures greater than approximately 1100 °C usually resulted in a degradation of the LEED pattern. Typically, the second order spot intensity was

reduced, and the background intensity increased. In these cases first order spot intensity usually remained strong. The quality of the (2x1) LEED patterns obtained upon annealing samples varied considerably, and no consistent trends were observed to account for the variability.

Samples exhibiting good reconstructions were then exposed to atomic hydrogen in an attempt to convert the surface back to a (1x1) configuration. Three pressure regimes were investigated: 10^{-6}-10^{-5} Torr, 10^{-3}-10^{-2} Torr and 1-10 Torr. Only at the highest pressures studied were we able to partially convert the surface back to a (1x1) state. Samples exposed to atomic hydrogen at the maximum pressure showed only very faint second order spots. Annealing of these samples to 1000 °C restored the (2x1) configuration. At the two lower pressure regimes studied little if any change was seen in the (2x1) LEED patterns upon addition of atomic hydrogen.

Given the difficulty in converting the surface back to a (1x1) configuration, all thermal desorption spectra were, perforce, from surfaces that had an indefinite degree of surface reconstruction. The three dosing regimes used in the LEED study were also used in the thermal desorption studies. Of the masses monitored during the course of the study, (2,13,14,15,16,18,26,27,28, and 44), desorption peaks were seen only for masses 2,15, and 26.

Figure 1 shows a series of hydrogen desorption spectra taken from a hydrogen dosed natural diamond surface. The sample was subjected to atomic hydrogen doses at fixed pressures and for a series of increasing times. A single desorption peak is evident at 900 °C. Figure 2 shows a similar series of hydrogen thermal desorption traces for the CVD homoepitaxial sample dosed at a pressure of $3x10^{-6}$ Torr. In this case two closely spaced hydrogen desorption peaks can be seen at 900 °C and at 1000 °C. It is apparent from both figures that extending the dosing time does not result in dramatically increased amounts of hydrogen desorbing from the surface. We also do not see any evidence for a shift in the desorption temperature as the coverage increases. The next series of figures shows thermal desorption spectra from the CVD diamond film after exposure to atomic hydrogen at the three pressure regimes used in the LEED study. Figure 3 shows that after exposure to atomic hydrogen at $1x10^{-5}$ Torr, hydrogen desorbs at 900 °C and perhaps a small amount of CH_3, but little evidence of C_2H_2. Figure 4 shows the sample after dosing at $2x10^{-3}$ Torr, a dosing pressure far higher than what is required to terminate the (2x1) surface. At this dosing pressure we now see clear evidence of desorbing methyl radicals (700 °C) and acetylene (600 °C). Although the sample has received an atomic hydrogen dose far in excess of what is required to saturate the (2x1) surface, LEED indicates the sample is in fact still in a (2x1) configuration. These two species are desorbing in significant quantities compared to the hydrogen desorption. The hydrogen desorption peak has broadened considerably after dosing at this pressure but the peak desorption temperature has not shifted. Figure 5 shows the sample after dosing at 3 Torr for 2700 seconds. In this case the sample has lost much of the (2x1) structure as seen in LEED but has not fully regained the (1x1) surface structure. The hydrogen desorption peak has remained at 950 °C. The methyl peak has shifted to approximately 800 °C and the acetylene peak has virtually disappeared.

Discussion

Surface reconstruction on the diamond (100) face has been reported previously (2,3). As noted by these authors, the reconstruction process was not always reproducible. For all of the newly polished surfaces used in the present study, some reconstruction was noted upon annealing. However, as indicated in the results, section not all surfaces fully reconstructed. Field emission SEM indicates the starting morphology for all the hand-polished surfaces was quite similar. If surface morphology is influencing the reconstruction, it is at a scale of less than 1000Å. Hamza et al. have suggested that adsorbed oxygen can affect the ability of the surface to reconstruct (3). Ex-situ measurements of samples show the presence of oxygen on the surface, some or all of which may have been added to the surface during the air transfer to the XPS system. No clear trend connecting the quantity of adsorbed oxygen and the quality of the reconstruction was observed. Other contaminants below the detection limit of XPS remain a possibility. Annealing at temperatures higher than required to establish the (2x1) structure appears to degrade the surface. The (1x1) pattern is still apparent but, as an increase in the background is observed, it is likely that the surface is becoming disordered and the (1x1) pattern is from the bulk.

Conversion of the (2x1) surface structure back to the original (1x1) structure appears very difficult. Extended dosing at high pressures is only partially successful at restoring the surface. In contrast, silicon (100) samples in the same chamber and under identical dosing conditions readily convert from the (2x1) state to the (1x1) state at dosing pressures of $1x10^{-6}$ Torr and at dosing times on the order of 1000 sec. For diamond samples in this pressure regime, we do not see conversion even after 2000 seconds at $5x10^{-6}$ Torr; a dose 10 times at great as used on silicon. This is not too surprising as the C-C bond strength at 83 kcal/mole is much greater than the Si-Si bond of 46 kcal/mole. Cluster calculations by Verwoerd indicate the diamond surface dimer bond is very resistant to attack by atomic hydrogen (5). The apparent stability of the dimer bond may also help explain results of the thermal desorption experiments described next, particularly the appearance of acetylene.

It appears difficult to maintain a well characterized surface during the course of thermal desorption experiments. The surface structure is evidently a function of sample history and it is difficult to return to a standard starting point. In the case of the thermal desorption experiments there may be several sites which are contributing to the hydrogen observed. LEED in this case is a very rough measure of surface characteristics. On a nominally (2x1) surface we find the hydrogen uptake saturates. By comparing this with data obtained from silicon samples under identical conditions, we find the quantity of hydrogen desorbed is consistent with monohydride coverage, or 1 hydrogen per carbon atom. Extended dosing does not significantly increase the hydrogen yield from the surface. The substrate which had received the homoepitaxial film showed two hydrogen desorption peaks only after film deposition. Before the film was deposited, a single peak is observed at 900° C. The desorption temperature does not appear to be coverage dependent. This indicates a first order reaction with fixed activation energy. A simple calculation using a standard frequency factor of 10^{13} gives an activation energy of 74 kcal/mole, which is considerably smaller than the C-H dissociation energy of 104 kcal/mole. First order kinetics are also found by Sinniah et al. for hydrogen desorption

from the monohydride phase on the silicon (100) surface (6). Along with first order kinetics, an activation energy was found which was much less than the dissociation energy for the Si-H bond.

As additional hydrogen is added to the saturated (2x1) surface we see the appearance of new desorption products, methyl radicals and acetylene. Since the dimer bonds resist attack by atomic hydrogen it may be possible for the dimer back bonds to be hydrogenated. If one or two of the back bonds were broken on the dimer unit, it would then be possible for the two carbon atoms to desorb as a unit, perhaps resulting in the acetylene production seen. Methyl radicals are also seen desorbing from the surface, but at a higher temperature. Since the two species desorb at different temperatures, one expects evolution from different sites. Mass 15 could be a fragmentation product of either ethylene or ethane. Mass 28 was monitored for ethylene species but given the large background seen at this mass it is difficult to discern a peak. No significant desorption products were seen at mass 27 either, which one would expect if large quantities of ethylene or ethane were desorbing. Given the size of the hydrocarbon desorption peaks relative to the hydrogen peak, it is clear that an appreciable fraction of a monolayer of carbon is desorbing from the (2x1) surface after extended dosing. It is not clear what sites the methyl radicals may be desorbing from. It seems likely that the methyl radicals are desorbing from dihydride sites.

If breaking of back bonds is occurring during hydrogen dosing, it seems likely that etching of the dimer units is also occurring on a continuous basis. If completed, we should see a reduction in amount of acetylene desorbed from the surface. At the highest hydrogen doses studied, the acetylene does in fact diminish dramatically. Methyl radicals, however, are still seen. Although the sample has moved closer to the (1x1) configuration as a result of the hydrogen dosing, the hydrogen desorption peak remains at 950°C. If desorption is occurring by processes similar to that on silicon, one would expect a peak to appear at a lower temperature corresponding to the desorption from the dihydride phase. Hamza et al. have results which indicate that both on the (100) and the (111) face of diamond, the surface reconstructs after the hydrogen desorbs (2,7). If there was little energy to be gained by formation of the dimer bonds on the surface, one would expect the desorption from the dihydride and the monohydride to occur near the same temperature.

Conclusions

The clean surface appears to saturate quite readily in the (2x1) configuration and hydrogen desorption from this phase follows first order kinetics. Conversion of a diamond (2x1) surface back to the (1x1) configuration by the addition of atomic hydrogen is difficult. It appears this is accomplished by hydrogenation of dimer back bonds and subsequent desorption of acetylene from the surface rather than by breaking of dimer bonds. Surfaces which show substantial reduction in the (2x1) surface phase after hydrogenation also show considerably reduced desorption of acetylene.

Acknowledgements

The authors wish to thank the Strategic Defense Initiative Organization/Innovative Science and Technology Office through the Office of Naval Research (N-00014-86-C-0460) for the financial support of this work.

REFERENCES

1. S. Matsumoto, Y. Sato, and N. Setaka, Carbon 19, 232 (1981).
2. A.V. Hamza, G.D. Kubiak, and R.H. Stulen, Surf. Sci. 237 35 (1990).
3. P.G. Lurie, and J.M. Wilson, Surf. Sci. 65, 453 (1977).
4. J.B. Posthill, R.A. Rudder, G.C. Hudson, D.P. Malta G.G. Fountain, R.E. Thomas, R.J. Markunas, T.P. Humphries, R.J. Nemanich, and D.R. Black, this proceedings.
5. W.S. Verwoerd, Surf. Sci. 108 153 (1981).
6. K. Sinniah, M.G. Sherman, L.B. Lewis, W.H. Weinberg, J.T. Yates, and K.C. Janda, Phys. Rev. Lett. 62 567 (1989).
7. A.V. Hamza, G.D. Kubiak, and R.H. Stulen, Surf. Sci. 206 L833 (1988).

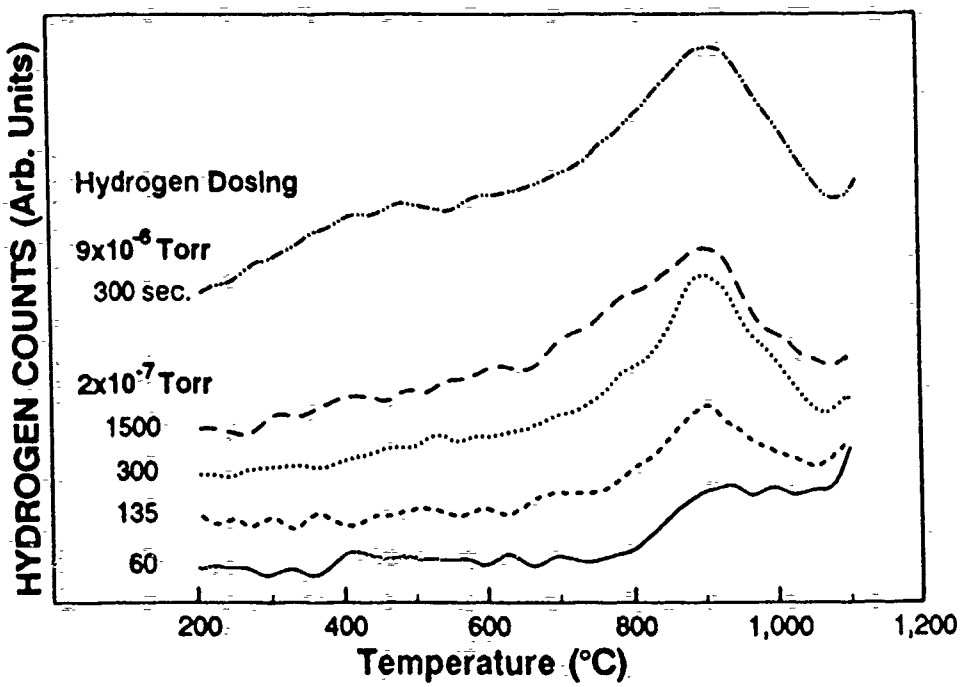

Figure 1. Thermal desorption spectra from natural diamond surfaces. An additional spectra was taken after dosing the sample at $9x10^{-6}$ torr with atomic hydrogen. The higher pressure is comparable to the dosing pressure used on the samples in Figure 2. Note that although the dose has increased by a factor of 3.5 between the sample exposed at $9x10^{-6}$ and the sample exposed for 1500 seconds at $2x10^{-7}$ torr, the magnitude of the desorption peaks is very close.

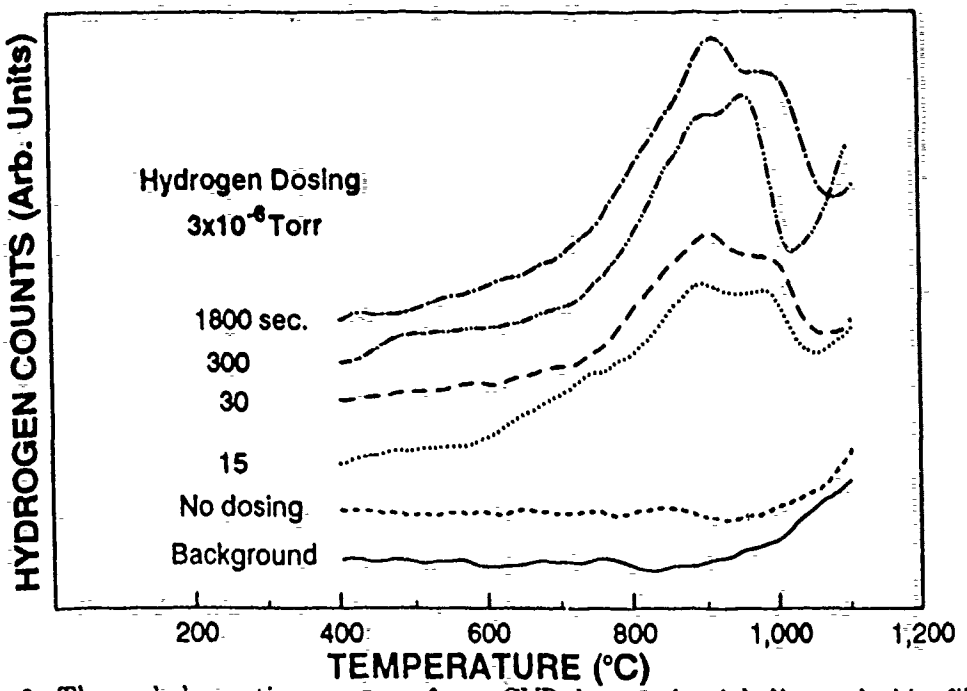

Figure 2. Thermal desorption spectra from CVD homoepitaxial diamond thin films deposited on natural diamond substrates. In addition to the hydrogen desorption spectra after dosing, a background spectrum is included where the sample was dosed but not placed adjacent to the aperture.

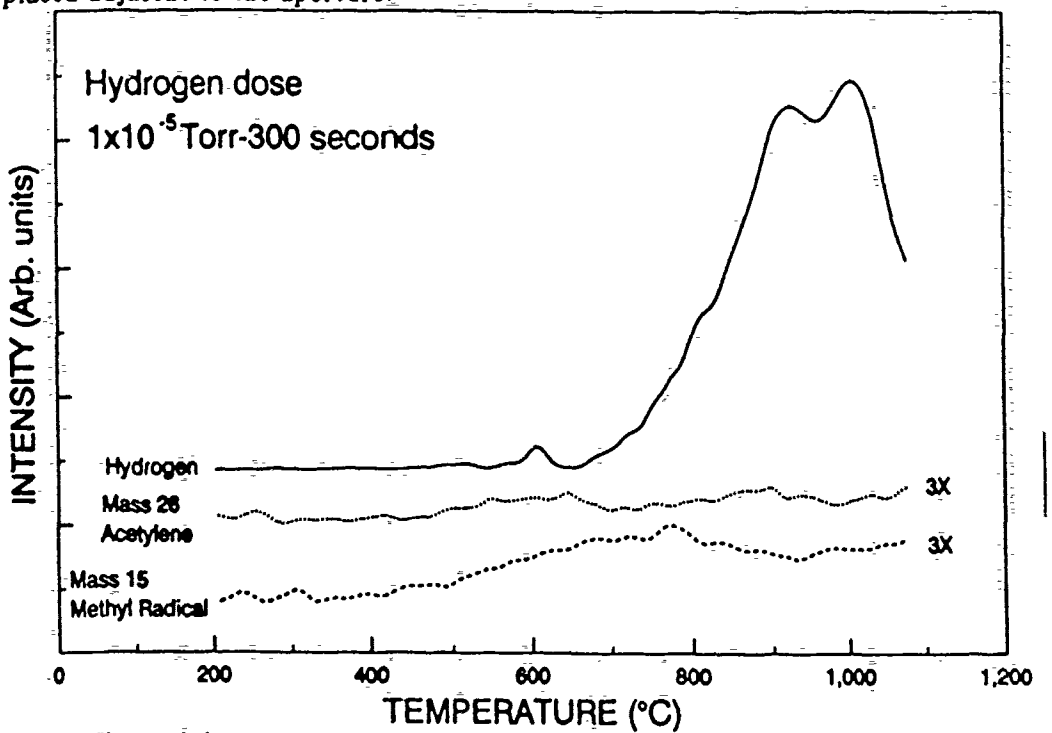

Figure 3. Thermal desorption spectra from CVD homoepitaxial diamond thin film after dosing at $1x10^{-5}$ torr. The vertical scale on masses 15 and 26 has been magnified by a factor of 3 to show detail.

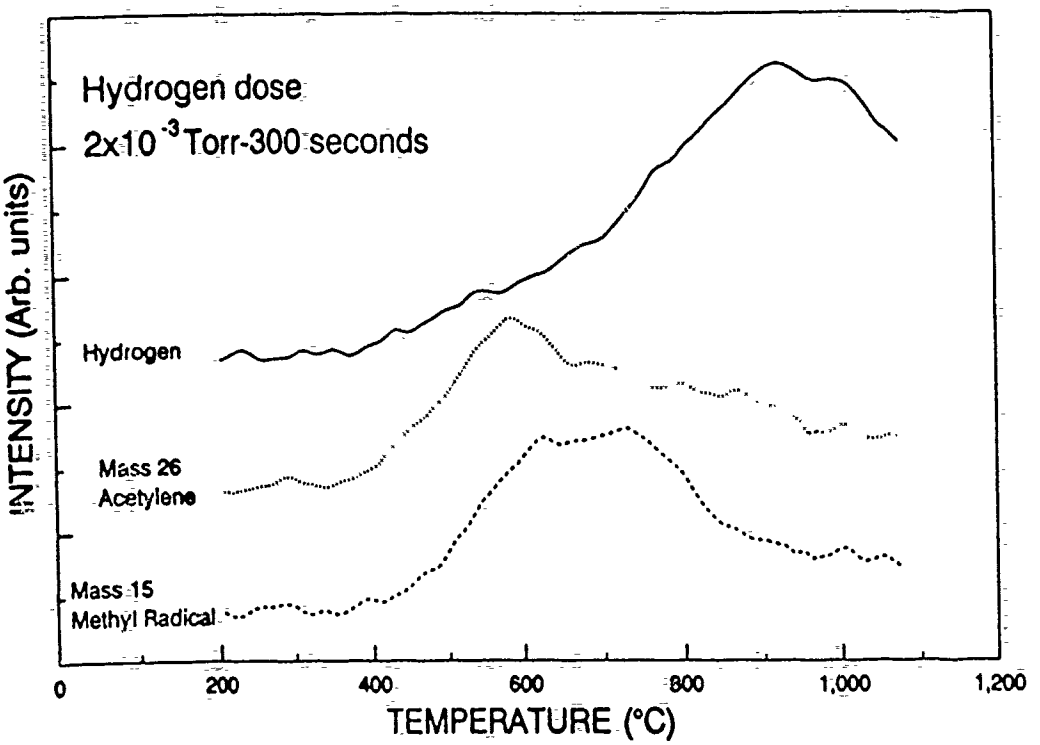

Figure 4. Thermal desorption spectra from CVD diamond film after hydrogen dosing at $2x10^{-3}$ torr. Note the large increase in methyl and acetylene production compared to Figure 3.

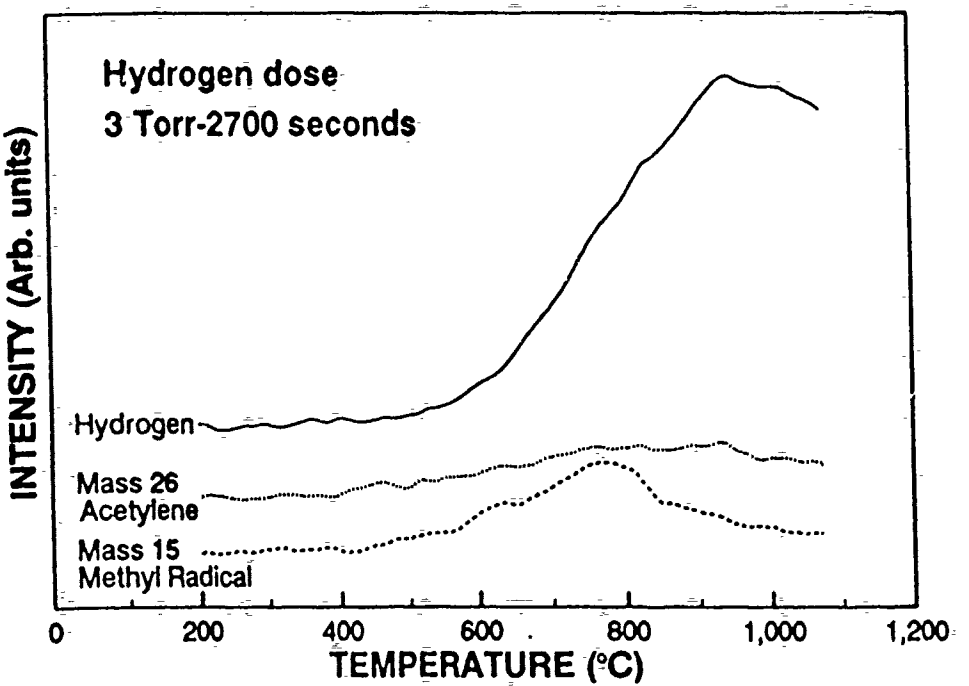

Figure 5. Thermal desorption spectra from CVD diamond film after hydrogen dosing at 3 torr. In this case the acetylene production is considerably reduced.

$F_2 - CH_4$ AND $H_2 - CF_4$ GAS INTERACTIONS ACROSS A HEATED GRAPHITE ELEMENT

R.A. Rudder, R.E. Thomas, G.C. Hudson, M.J. Mantini, and R.J Markunas
Research Triangle Institute, P.O.Box 12194, Research Triangle Park, NC 27709

ABSTRACT

We have investigated diamond film formation using mixed hydrogen-halogen chemistries at sub-atmospheric pressures. This work has been implemented in two reduced pressure cells. One cell contained a heated graphite element upon which reactant gasses were passed. Only thermal activation was used in this reduced pressure cell. Quadrupole mass spectroscopy was used to identify reaction products in the cell. The other cell was a low pressure rf-plasma assisted chemical vapor deposition system. Gasses were admitted to this cell which showed no thermal activation in the thermal cell. It was found that F_2 is activated in the thermal cell and can participate in reactions both in the gas phase and at the graphite surface. HF and $C_2F_2H_x$ were observed as by-products of $F_2 - CH_4$ gas interactions near the graphite oven. Carbon films that were deposited on nearby substrates proved not be diamond. Activation of $H_2 - CF_4$ in the thermal cell was not observed even at temperatures as high as 1000 ° C. Plasma activation, on the other hand, does show evidence for HF and C_2H_2 formation from the H_2 - CF_4 gas system. With plasma activation of $H_2 - CF_4$ gas system, diamond deposition on as-received Si wafers without any ex situ treatment of the surface to enhance diamond nucleation is possible.

Introduction

Recent work by Patterson et al.(1) and previous work by Rudder et al.(2) has shown that diamond deposition from a fluorine-based environment is possible. Patterson exploited the use of mixed fluorine-hydrogen chemistries (i.e., F_2 and CH_4) to form solid carbon through a proposed reaction of:

$$CH_4 + 2F_2 \rightarrow C_{(s)} + 4HF \quad (1)$$

This reaction would be more exothermic than a corresponding hydrogen-based reaction involving CH_4 and H_2. The hot zone of the Patterson-type

reactor operated between 700 and 950 °C, and diamond growth occurred only in regions of the reactor where the temperature was between 250 and 750 °C. Mixtures of either H_2 and CF_4 or F_2 and CH_4 were reported to deposit diamond.

Experimental Apparatus and Approach

To gain insight into the fluorine-based process, we have performed a quadrupole mass spectroscopy of F_2/CH_4 and H_2/CF_4 gas interactions as a function of temperature of the graphite surface. This work has been implemented in two reduced pressure cells. One cell contained a heated graphite element upon which reactant gasses were passed. Only thermal activation was available in this reduced pressure cell. The other cell was a low pressure rf-plasma assisted chemical vapor deposition system. Gasses were admitted to this cell which showed no activation in the thermal cell.

The thermal work was performed in an UHV compatible chamber that is evacuated by a corrosive series, 1000 l/s turbomolecular pump. Gases are admitted into the chamber using mass flow controllers. The pressure in the chamber is maintained at 0.500 Torr for $F_2 - CH_4$ or $H_2 - CF_4$ gas work described here. A graphite resistive heater is enclosed in the chamber as well as a sample heater stage whereby growth attempts, independent of the graphite resistive heater, can be assessed. The graphite heater is machined from a dense, fine-grain graphite and is not highly oriented pyrolytic graphite. A mass quadrupole operating at low emission (0.25 mA) is used to sample the gases exiting the reactor. Changes in the gas composition as a function of substrate temperature or the graphite heater temperature are monitored.

The plasma activated cell was a low pressure rf-plasma assisted chemical vapor deposition system which has been used for the growth of diamond from H_2 - CH_4 mixtures(3). The reactor cell consists of a stainless steel, 150 mm conflat flange, 6-way cross to which the reactor tube, pumps, control orifice valve, vacuum gauges, mass spectrometer, and load lock are appended. The vacuum system is evacuated by a Balzers 500 l/s corrosive series turbomolecular pump. The base pressure of the reactor is 1.0×10^{-7} Torr. The heater stage is comprised of alumina standoffs separating the graphite susceptor from a graphite serpentine resistive heater. The reaction tube consists of a double-walled 50 mm inside diameter quartz tube sealed to the stainless chamber by compression viton o-ring seals. The reactor tube is water cooled to maintain the water temperature at 15 °C. An 8 mm water-cooled copper tube formed into a 3-turn helix 100 mm long provides the inductive coupling from the rf generator to the discharge. Wall deposits, for a limited time, can protect the quartz tube from erosion by fluorine based processes.

Experimental Results in Thermal Cell

The interactions of F atoms with both solid carbon such as graphite and with gaseous carbon such as CH_4, a graphite strip heater were studied in the thermal cell. By adjusting the current through the graphite element, the reactions of F_2 and/or F with the densified graphite were monitored as a function of temperature. One advantage in using a graphite heater to study the F_2/CH_4 gas interactions is that reactions of fluorine with graphite have been previously studied(4) so there exists comparative information. A second advantage to the graphite heater is that it avoids questions of metal catalysis reactions. Two difficulties with the graphite heater are memory effects from gasses absorbing in the porous graphite and delocalization of the hot zone across the machined graphite. This results in some areas of the heater operating about 100°C colder than the heater center. To minimize the memory effects, the heater was degassed at high temperatures before setting the temperature for each data point.

Fluorine reactions with the heated graphite were monitored by admitting the F_2 without CH_4 into the thermal cell. At elevated temperatures, fluorine reacted with the graphite to form CF_4. The CF_4 formation was monitored in the mass quadrupole through the mass peak at 69 arising from CF_3. CF_3 is the dominant fragment in the ionizer when CF_4 is introduced. Figure 1 shows the observed CF_3 mass counts in the reactor as a function of the graphite cell temperature. The CF_4 production is maximum at 600°C and is observed to decrease for temperatures in excess of 950°C. The decrease in CF_4 production below 600°C is probably a consequence of the formation of solid graphite fluoride. The temperature dependence is convoluted by the fact that there is a substantial temperature variation ± 100°C across the graphite heater element.

After observing the CF_4 production from the hot cell with only F_2 (admitted as 1% F_2 in He), CH_4 was introduced into the hot cell. Upon introduction of CH_4 into the hot fluorine, the CF_4 production decreased. Fluorine interactions with the CH_4 in the gas phase apparently depleted the gas phase of fluorine, resulting in a lower incident flux of F atoms to the graphite surface and, consequently, a lower production rate of CF_4. This is the first evidence for $F_2 - CH_4$ gas phase interactions. Besides the reduction in CF_4 production, the introduction of CH_4 into the hot fluorine resulted in production of HF and $C_2F_2H_x$ molecules. Figure 2 shows the production of those molecules as a function of the graphite temperature. Both exhibit a maximum in production around 900°C. The temperature dependence for the HF production is more pronounced than the temperature dependence for the $C_2F_2H_x$ production.

This work suggests that the proposed reaction of Patterson et al. for solid carbon production via equation (1) is basically correct. Our observations of graphite gasification and the formation of HF and $C_2F_2H_x$ suggests that the reaction in equation (1) should be extended.

$$2F_2 + CH_4 \rightarrow C_{solid} + 4HF \qquad (700\,^\circ C)$$

$$4F_2 + 2CH_4 \rightarrow C_2H_2F_2 + 6HF \qquad (700\,^\circ C)$$

$$2F_2 + C_{graphite} \rightarrow CF_4 \qquad (500 - 700\,^\circ C)$$

In a similar manner, the H_2 - CF_4 system was evaluated in the thermal cell. At the pressure of 0.50 Torr, no evidence of by-product formation was observed for temperatures below 1000 °C. Temperatures higher than 1000 °C and pressures higher than 0.50 Torr were not evaluated. We assumed that temperatures under 1000 °C are not sufficient to produce H atoms from the H_2 or F atoms from the CF_4. Consequently, the H_2 - CF_4 gas system in this pressure and temperature range does not react with the graphite to produce gasification products, nor do they react with each other to form HF molecules.

Experimental Results in Plasma Cell

As a consequence of the inactivity of the H_2 - CF_4 in the thermal cell, gas mixtures of H_2 and CF_4 were admitted into the low pressure rf plasma assisted chemical vapor deposition system. Details of that work are being submitted elsewhere(5). Briefly, dense nucleation of polycrystalline diamond films on Si(100) substrates has been accomplished without the use of any surface pre-treatments such as diamond scratching, oil-coating, or diamond-like carbon predeposition. Films deposited at 5 Torr at 850 °C, using an 8% CF_4 in H_2 mixture, show dense nucleation, well-defined facets, and crystallite sizes ranging from 500 - 10,000 Å. Figure 3 shows scanning electron micrographs of the diamond surface and a cleaved cross-section. Some roughening of the Si substrate is observed from the cleaved section suggesting that the Si surface underwent some chemical modification prior to or during diamond nucleation. X-ray photoelectron spectroscopy show the films to be diamond with no major chemical impurity and no detectable graphitic bonding. Besides carbon, fluorine is detected in the x-ray photoelectron spectrum. A high resolution spectrum of the C 1s line shows that some carbon is bound to fluorine on the surface as exhibited by a distinct feature at 288 eV, removed from the C-C bonding at 283 eV. A high resolution spectrum of the C 1s region is shown in Figure 4. The graphite $\pi - \pi^*$ plasmon is not present in the spectrum. The 34 eV bulk diamond plasmon is clearly present, but not shown in the high-resolution spectrum. A pronounced 1332 cm^{-1} Raman line was observed from the polycrystalline films along with a broad

band at 1500 cm^{-1}.

Quadrupole mass spectroscopy of the gases downstream from the plasma discharge reveals that the CF_4 - H_2 plasma converts the carbon tetrafluoride into HF and C_2H_2. No fluoromethane groups were observed. Given that, after 15 min into the plasma process, no fluorocarbon groups were detectable in the mass spectrum, the generation rate of HF and C_2H_2 must have been equal to the gas flow of CF_4 into the reactor, 3.2 sccm.

Preliminary data indicates that this process is applicable to substrates other than silicon. This process will have important applications in areas where surface pretreatments, such as diamond powder, are not viable. In particular, this process may prove invaluable to those workers developing heteroepitaxy. With conventional methane-based processes, nucleation is inhibited on substrates other than diamond and c-BN. This process may allow heteroepitaxial studies to be undertaken on substrates whereby previously there has been little diamond nucleation.

Acknowledgements The authors wish to thank the Strategic Defense Initiative Organization/Innovative Science and Technology Office through the Office of Naval Research (N-00014-86-C-0460) for the financial support of this work.

REFERENCES

(1) Donald E. Paterson, Benjamin J. Bai, C. Judith Chu, Robert H. Hauge, and John L. Margrave, "Halogen-Assisted Chemical Vapor Deposition", presented at the second International Conference on the New Diamond Science and Technology, Washington, DC(USA), September 23-27, 1990.

(2) R.A. Rudder, J.B. Posthill, R.J. Markunas, Electronics Lett. 25, 1220 (1989).

(3) R.A. Rudder, G. C. Hudson, Y. M. LeGrice, M.J. Mantini, J.B. Posthill, R.J. Nemanich, and R.J. Markunas, Mat. Res. Soc. EA-19

(4) D.E. Rosner and J. Strakey, J. Phys. Chem. 77, 690 (1973).

(5) R.A. Rudder, G.C. Hudson, J.B. Posthill, R.E. Thomas, and R.J. Markunas, submitted to Appl. Phys. Lett.

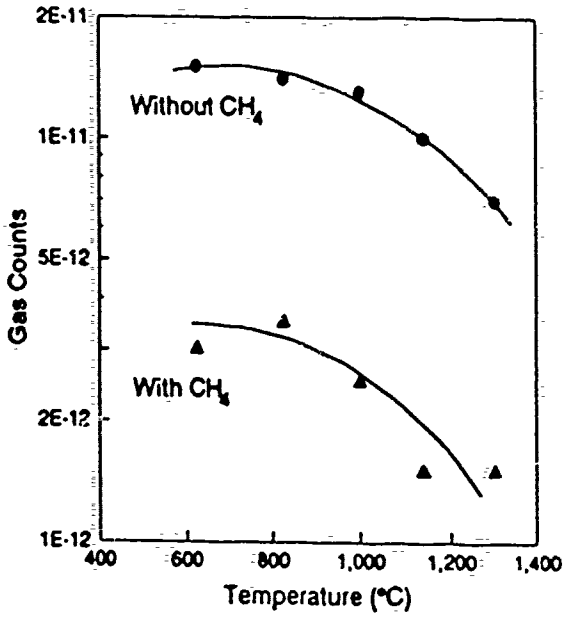

Figure 1. Observed CF_3 counts in the mass spectrometer as a function of the graphite heater temperature. Notice that the introduction of CH_4 into the graphite hot zone diminishes the CF_4 production.

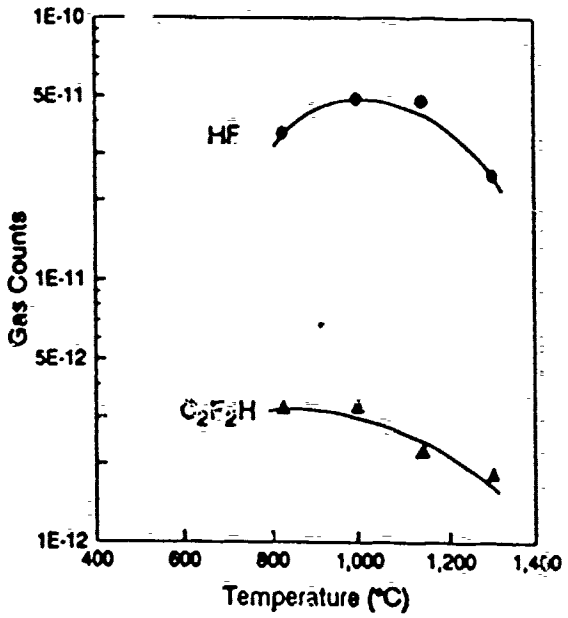

Figure 2. Dependence of by-product production on graphite heater temperature.

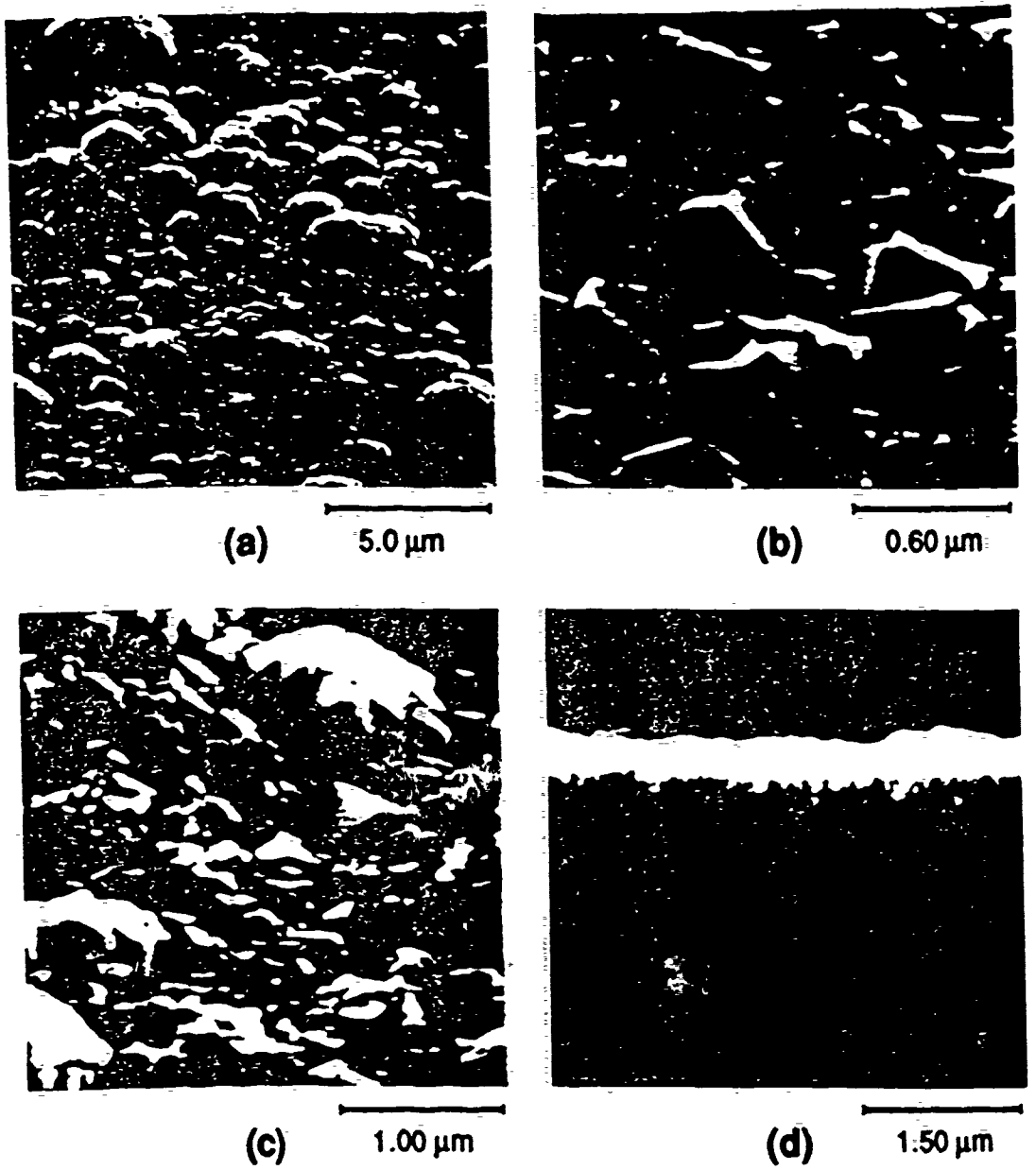

Figure 3. SEM micrographs of a polycrystalline diamond film deposited from the H_2 - CF_4 process.

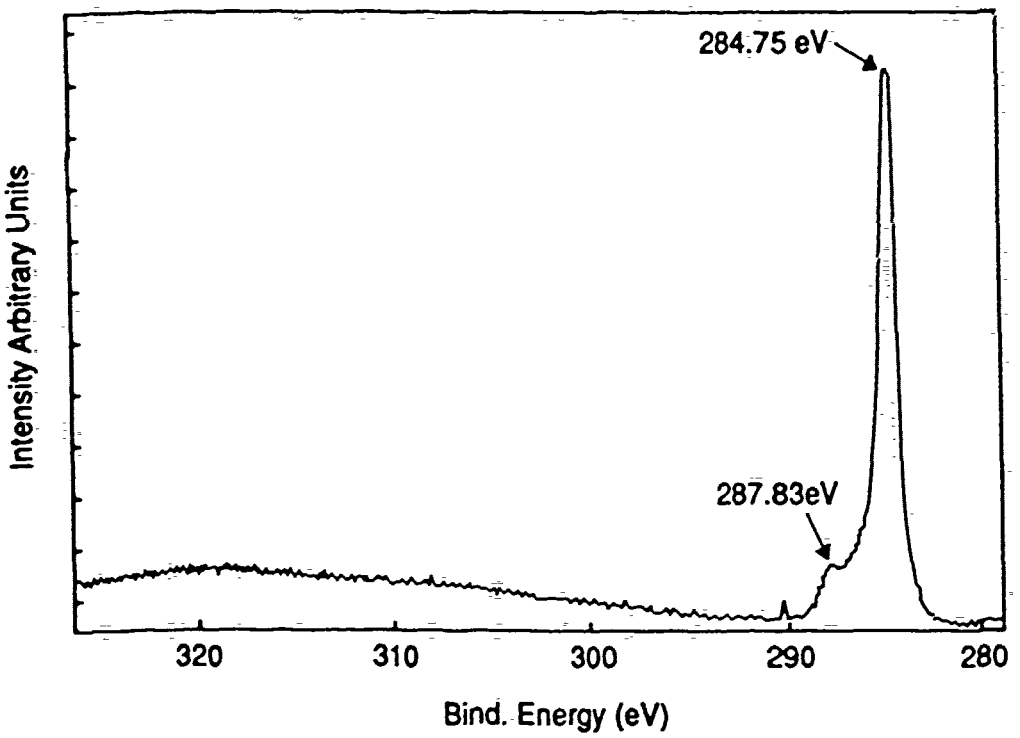

Figure 4. A high resolution x-ray photoelectron spectrum of the C 1s line.

ACETYLENE PRODUCTION IN A DIAMOND-PRODUCING LOW PRESSURE rf-PLASMA ASSISTED CHEMICAL VAPOR DEPOSITION ENVIRONMENT

R.A. Rudder, G.C. Hudson, J.B. Posthill, R.E. Thomas, and R.J Markunas
Research Triangle Institute, P.O.Box 12194, Research Triangle Park, NC 27709

R.J. Nemanich, Y.M. LeGrice, and T.P. Humphreys
Department of Physics
North Carolina State University, Raleigh, NC 27695-8202

ABSTRACT

We have examined using quadrupole mass spectroscopy the production of acetylene molecules under diamond growth conditions wherein no acetylene was introduced. There are two pathways available for the production of acetylene. One path for acetylene production is through conversion of CH_4 into C_2H_2 in the high temperature plasma region. The other path for acetylene production is through gasification of the graphite. In the pressure range from 1 - 10 Torr using a rf plasma discharge, the graphite gasification is the dominant path and the diamond deposition rate appears to correlate fairly well with the acetylene concentration in the reactor. The correlation can be understood by considering the acetylene production rate to be proportional to the atomic hydrogen flux to the graphite susceptor and, hence, to the atomic hydrogen flux to the diamond growth surface.

Introduction

Many workers are studying the importance of acetylene and methyl radicals in the vapor phase growth of diamond. Techniques such as infrared diode laser absorption spectroscopy and multiphoton ionization have been used to examine the gaseous environment of the diamond deposition(1). Other workers have used isotopic labeling to identify the parentage of carbon atoms deposited as diamond(2). In this work, we have used quadrupole mass spectroscopy to monitor acetylene production during diamond deposition in a low pressure rf-plasma chemical vapor deposition environment. We find that there are two channels for acetylene production, one via conversion of CH_4 into C_2H_2 and second via gasification of graphite into C_2H_2. By realizing that a requirement for graphite gasification is the atomic hydrogen flux to the graphite surface. mass quadrupole spectroscopy of the gasification products has been able to demonstrate that the diamond deposition rate is proportional to the atomic hydrogen flux.

Experimental Approach and Results

Diamond depositions have been accomplished in a low pressure rf plasma assisted chemical vapor deposition system using 1% CH_4 in H_2 gas at pressures from 1 - 10 Torr. Details of that reactor and the growth process have been previously reported(3). The vacuum system for diamond deposition is shown schematically in Figure 1. It consists of a stainless steel 150 mm conflat flange 6-way cross upon which the reactor tube, pumps, control orifice valve, vacuum gauges, quadrupole mass spectrometer, and load lock are appended. Samples are introduced into the reactor on a graphite carrier/susceptor through a vacuum load lock, transferred horizontally onto a heater stage. and raised vertically into the quartz reaction tube. The reaction tube consists of a double-walled 50 mm inside diameter quartz tube sealed to the stainless chamber by compression viton o-ring seals. The reactor tube is water cooled through the use of a heat exchanger which maintains the water temperature at 15 °C. A 8 mm water-cooled copper tube formed into a 3-turn helix 100 mm long provides the inductive coupling from the rf generator to the discharge. The rf power output from a power amplifier tube couples to the plasma using a LC resonant circuit with the plasma coil constituting the inductive component. The vacuum system is evacuated by a Balzers 500 l/s corrosive series turbomolecular pump. The pressure of the reactor is 1.0×10^{-7} Torr prior to introducing the reactant gasses.

Conditions for diamond growth are given in Table I over the presure range from 1 - 10 Torr. Note that the temperature of the hydrogen plasma has been calculated from the relative emission intensities of the atomic hydrogen Balmer series assuming a Boltzman distribution and collisionless lifetimes. These assumptions may be in error, but this calculation allows some internal standard for the power input to the plasma.

Table I

Pressure	Flow rate (sccm)	Estimated rf power (w)	T_{plasma} (K)
1	1.3	400	3420
3	3.8	660	3350
5	6.3	1000	3200
7	8.8	1800	3200
10	12.5	2400	3270

One notices that the pressure in this series is varied by maintaining a constant pumping speed and reducing the gas flow into the reactor. The estimated plasma temperature remains constant throughout this pressure range despite

the 6-fold increase in power input. Without this increase in power at the higher pressures, it would not be possible to maintain the atomic hydrogen emission. This increase in applied power also increases the substrate temperature. The substrate temperature varies from ≈650 °C at 1.0 Torr to ≈850 °C at 10 Torr.

Following deposition, films were analyzed using scanning electron microscopy (SEM) and Raman scattering spectroscopy. Cleaved sectional analysis in the SEM was used to ascertain diamond deposition rates at the different pressures. We assumed the deposition rate was linear in time. The silicon substrates used in this work were diamond polished prior to introduction into the reactor to provide immediate nucleation sites.

SEM micrographs show that the deposited films are polycrystalline showing well-defined faceting. The crystallite sizes vary from 0.5 - 2.5 μm. The crystallites appeared to have nucleated at point sites upon which growth proceeded 3-dimensionally into a continuous film. Raman spectra for the complete series are given in Figure 2. All samples display a 1332 cm^{-1} diamond Raman line. Samples grown at lower pressures show more non-diamond bonding. It is not clear at this point if the appearance of the non-diamond bonding components (i.e. the appearance of Raman features between 1500 and 1600 cm^{-1}) is due to a reduction in pressure or a reduction in substrate temperature. It is clear that all conditions produced diamond from the gas phase using the low pressure rf-plasma system.

The environment of the diamond growth was probed by mass spectroscopic analysis of gasses downstream from the plasma region. Samples were positioned near the rf coil on a graphite susceptor. By comparing the C_2H_2 production observed with the graphite susceptor removed from the discharge tube to the C_2H_2 production when the susceptor was positioned near the rf coil, one can distinguish CH_4 conversion to C_2H_2 in the gas phase from gasification of the graphite to C_2H_2 at the susceptor surface. (It should be noted that these experiments were performed when the plasma tube was fairly clean of carbon deposits. The graphite susceptor represents the largest source of solid carbon exposed to the plasma.) Figure 3 shows the conversion of CH_4 to C_2H_2 as a function of total pressure when the graphite susceptor is *not* present in the reactor. This figure shows a nearly constant ratio of CH_4 to C_2H_2 across the pressure series. Given that two CH_4 molecules are necessary for C_2H_2 production, we conclude that approximately 60% of the CH_4 is converted into C_2H_2. Figure 4 shows the observed C_2H_2 production when the graphite susceptor is inserted 3.0 mm below the rf coil with 1% CH_4 in H_2 discharge. There is a pronounced pressure dependence to the C_2H_2 production. At 3 Torr, there is approximately 4 times more C_2H_2 partial pressure in the reactor with the graphite susceptor present than there was with the graphite susceptor absent. More C_2H_2 is produced at 3 Torr by graphite gasification than is produced by CH_4 conversion into C_2H_2.

It is interesting to compare the diamond deposition rate with the C_2H_2 production rate. Figure 5 shows the growth rate as a function of pressure for this series. We find that the deposition rate is a maximum for a pressure of approximately 3 Torr. A comparison with Figure 4 shows that the deposition rate and the C_2H_2 production rate both show a similar dependence on reactor pressure with the highest deposition rate and the highest C_2H_2 production rate occuring at 3 Torr.

Discussions and Conclusions

This work shows an apparent correlation between the deposition rate of diamond and rate of gasification of the graphite susceptor into C_2H_2. Perhaps, the growth rate of diamond is inhibited by graphitic sites which must be removed before diamond can propagate. Hence, growth conditions which rapidly gasify graphite, remove graphitic sites from the diamond surface allowing diamond growth to propagate. Mucha et al.(4) used similar arguments to explain higher effective growth rates in microwave CVD experiments when alternating cycles of H_2 and CH_4 were introduced into the reactor. Alternatively, the C_2H_2 radical may be promoting diamond growth as Frenklach et al.(5) have suggested. Thus, higher concentrations of C_2H_2 in the gas phase may be responsible for the higher growth rate.

The work of Balooch and Olander(6) yields considerable insight into the data presented in this paper. Balooch and Olander showed that the gasification products observed when atomic hydrogen interacts with pyrolytic graphite are distinctly different depending on the temperature of the graphite. At temperatures below 550°C, the primary product was CH_4. At temperatures above 900°C, the primary product was C_2H_2. Balooch and Olander argued that in the intermediate temperature range H atoms recombined on the pyrolytic graphite surfaces without substantial graphite gasification. In the pressure series reported in this paper, the graphite susceptor is certainly above 550°C. We, as Balooch and Olander, do observe C_2H_2 as a by-product of atomic H with graphite. We are able to deposit diamond films in the intermediate temperature range where atomic hydrogen is not as efficient in dissolving graphite. It should be noted that the flux of atomic hydrogen present to a diamond CVD growth surface is orders of magnitude higher than the fluxes used by Balooch and Olander. Consequently, graphite removal from a diamond CVD growth surfaces with atomic H is undoubtedly possible.

The production of C_2H_2 from a graphite surface at elevated temperatures will be proportional to the atomic hydrogen flux. If one interprets the C_2H_2 production rate shown in Figure 4 as proportional to the atomic hydrogen flux to the graphite surface and hence to the diamond CVD growth surface, then one

concludes that the atomic hydrogen flux to the growth surface is a strong function of pressure. Hence, the correlation between diamond growth rate and acetylene production is more conc 'y a consequence of the differing atomic hydrogen fluxes. The higher fluxes o. atomic hydrogen dissolve graphite and promote diamond bonding. These results are strong support for the work of Yarbrough(7) showing that at high atomic hydrogen concentrations diamond precipitated as the stable phase.

Acknowledgements The authors wish to thank the Strategic Defense Initiative Organization/Innovative Science and Technology Office through the Office of Naval Research (N-00014-86-C-0460) and the Office of Naval Research (N00014-90-J-1707) for the financial support of this work.

REFERENCES

(1) F.G. Celii, P.E. Pehrsson, H.-T. Wang, and J.E. Butler, Appl. Phys. Lett. 52 , 2045 (1988).

(2) C. Judith Chu, Mark P. D'Evelyn, Robert H. Hauge, and John L. Margrave, J. Mat. Res. 5, 2405 (1990).

(3) R.A. Rudder, G. C. Hudson, Y. M. LeGrice, M.J. Mantini, J.B. Posthill, R.J. Nemanich, and R.J. Markunas, Mat. Res. Soc. EA-19 , 89 (1989).

(4) J.A. Mucha, D.L. Flamm, and D.E. Ibbotson, J. Appl. Phys. 65, 3448 (1989).

(5) Michael Frenklach and Hai Wang, Phys. Rev. B 43, 1520 (1991).

(6) M. Balooch and D.R. Olander, J. Chem. Phys. 63, 4772 (1975).

(7) Walter A. Yarbrough, Mat. Res. Soc. Symp. Proc. 162, 75 (1990).

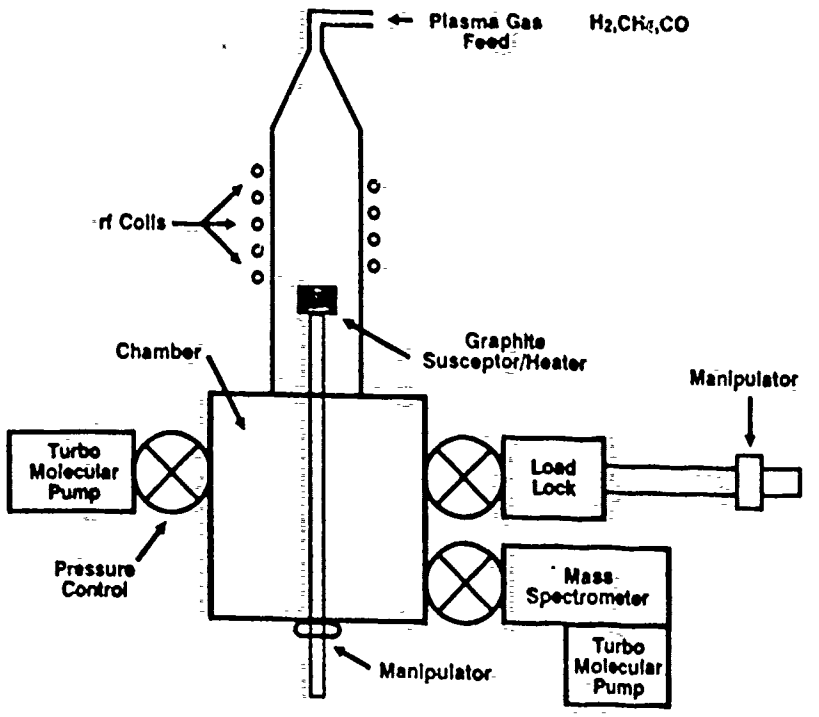

Figure 1. Schematic of low pressure rf-plasma assisted chemical vapor deposition system.

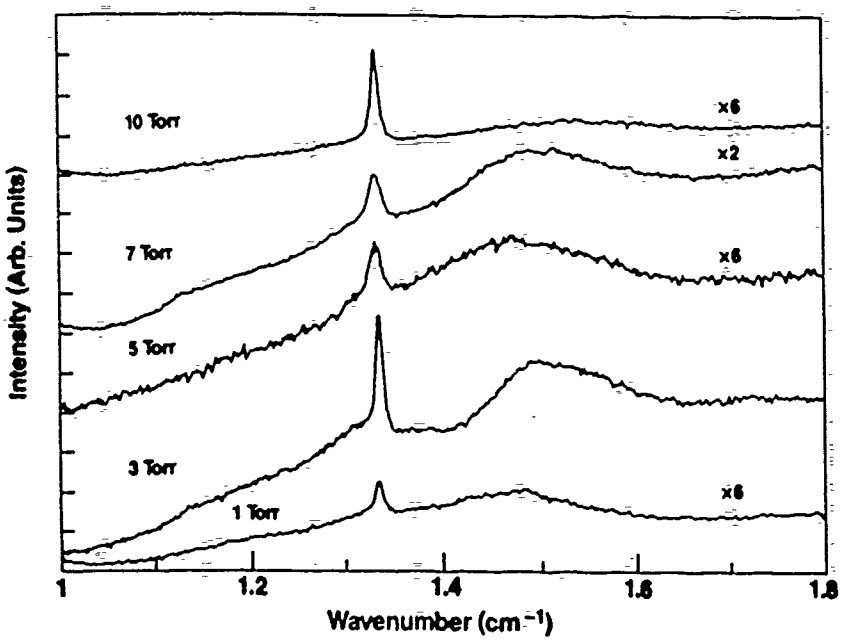

Figure 2. Raman spectra for diamond films deposited from 1 to 10 Torr using 1% CH_4 in H_2.

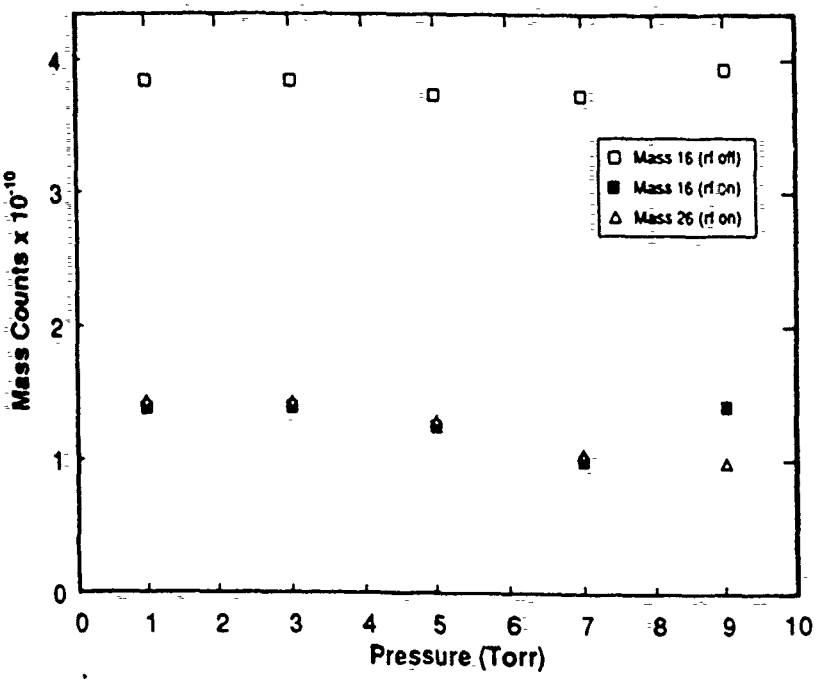

Figure 3. Conversion of CH_4 into C_2H_2 without the graphite susceptor in the reactor.

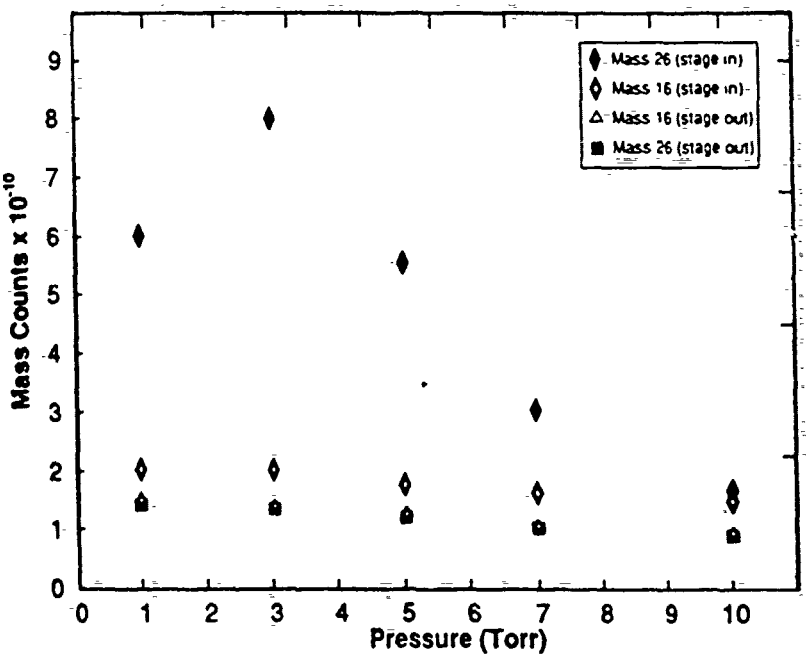

Figure 4. Production of C_2H_2 in the growth reactor as a function of pressure with the graphite susceptor in place.

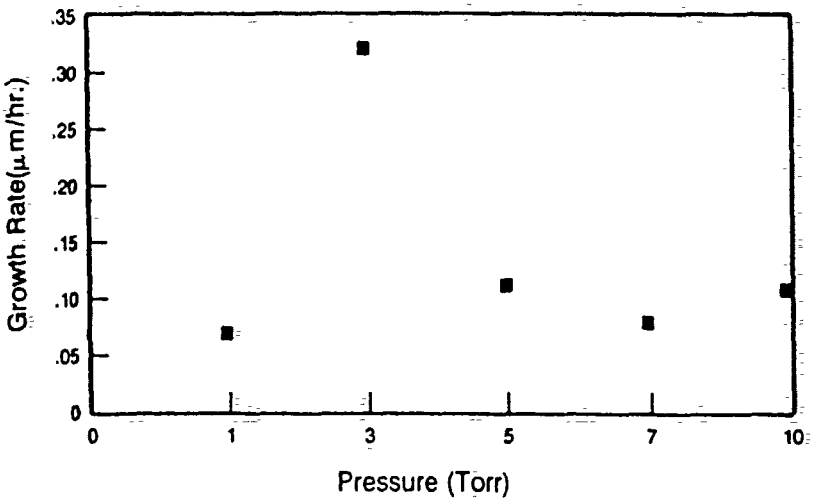

Figure 5. Diamond deposition rate as a function of pressure. Thickness values were obtained from SEM micrographs of cleaved sections.

SUBSTRATE EFFECTS AND THE GROWTH OF HOMOEPITAXIAL DIAMOND (100) LAYERS USING LOW PRESSURE rf PLASMA-ENHANCED CHEMICAL VAPOR DEPOSITION

J.B. Posthill, R.A. Rudder, G.C. Hudson, D.P. Malta,
G.G. Fountain, R.E. Thomas, and R.J. Markunas
Research Triangle Institute, Research Triangle Park, NC 27709-2194

T.P. Humphreys and R.J. Nemanich
Department of Physics
North Carolina State University, Raleigh, NC 27695-8202

D.R. Black
National Institute of Standards and Technology, Gaithersburg, MD 20899

ABSTRACT

The technological evaluation of commercially-available, single crystal diamond substrates for homoepitaxial diamond growth is presented. Surface topographies of insulating diamonds (types Ia, IIa, and Ib) are shown, and microstructural comparisons are examined with X-ray topography. Wet chemical and mechanical cleaning procedures are briefly reviewed. The effect of the starting substrate on the resultant homoepitaxial diamond film can be partially mitigated by the proper choice of substrate, appropriate cleaning protocol, and the use of a well-qualified diamond deposition technology.

Introduction

The thermal and electrical properties of diamond make it an excellent candidate for electronic applications. A number of significant problems must be overcome before the potential of diamond can be realized. While suitable heteroepitaxial substrates have not been developed yet, the fabrication of diamond transistors on natural diamond substrates allows testing and evaluation of diamond electronics [1]. One problem arising in the fabrication of diamond devices on diamond is the quality of the natural diamond substrates. Recent studies indicate that X-ray topography is a potentially valuable technique for characterizing structural defects in diamond single crystal substrates [2]. Selection of high quality diamond substrates is imperative to the growth of high mobility homoepitaxial diamond layers. In order to achieve the highest electrical quality diamond films, growth techniques may have to be developed which deposit epitaxial layers without replicating the crystalline defects commonly found in diamond single crystals.

This paper presents technological results accumulated over the last two years that pertain to the quality of commercially-available single crystal

diamond substrates, the cleaning of these substrates, and the resultant homoepitaxial diamond growth by low pressure rf plasma-enhanced chemical vapor deposition (PECVD). Both uniform coverage and selective-area diamond homoepitaxy are described.

Experimental Procedures

Natural type Ia and IIa and synthetically-produced type Ib diamond single crystals have been evaluated for their suitability for diamond homoepitaxy. Cutting and polishing to nominal (100) orientation were performed commercially by the vendors, and analysis has included scanning electron microscopy (SEM) [equipped with a field emission gun] on uncoated diamond substrates. X-ray topography [3], using near-parallel and monochromatic X-rays prepared from synchrotron radiation, has been used to evaluate the microstructure of selected type Ia, IIa, and Ib single crystal diamonds (not necessarily cut and polished to a specific orientation).

Two different chemical cleaning methods were utilized. Diamond substrates were cleaned with the RCA cleaning technique [4], which has found wide-spread use in silicon integrated circuit fabrication, or with sequential exposure to boiling CrO_3/H_2SO_4 solution (glass cleaning solution) for 15 minutes followed by boiling aqua regia for 15 minutes followed by a dip in 10:1 H_2O:HF solution and complete deionized water rinse. The efficacy of swabbing to remove particulates has also been evaluated. Cotton-tipped swabs were used in deionized water.

Homoepitaxial diamond growth was accomplished using a 13.56 MHz inductively-coupled plasma-enhanced chemical vapor deposition (PECVD) system as described in more detail elsewhere [5]. Briefly, the system is UHV-compatible and the nominal conditions used were: 1% CH_4 in H_2 or 1:2 mixture of 2% CO in H_2 and 1% CH_4 in H_2, total gas flow = 20-30 sccm (32.2-48.3 Pa-L-s^{-1}), pressure = 5.0 Torr (667 Pa), temperature = 500-800 °C, and rf power $\simeq$ 1.5kW. The homoepitaxial diamond films have been characterized with SEM and Raman spectroscopy.

Results and Discussion

Diamond Substrates

Features have been observed on the surfaces of commercially-supplied diamond substrates which might inhibit high quality epitaxial growth. Figure 1 shows a series of SEM micrographs from several as-received natural Type IIa diamond (100) substrates (size: 4 × 4 × 0.25 mm). It can be seen that the surface topographies do vary from substrate to substrate, and some are clearly "better" than others. However, the fine unidirectional scratches are observed on all substrates of this size. Commercially-produced synthetic, type Ib diamonds can also have surface topographies that may influence subsequent

epitaxy (Figure 2). However, it must be borne in mind that a less than perfectly smooth surface topography only indicates that the polishing process needs optimization and does not necessarily imply that the bulk of the substrate is microstructurally defective. This has been shown by electron-beam-induced current (EBIC) imaging of natural semiconducting type IIb diamonds in the SEM, where it has been seen that the surface scratches bear no relationship to subsurface microstructural defects that are nonradiative recombination sites [6].

The extent of microstructural defects in a diamond substrate is perhaps a more crucial issue pertaining to the attainment of low-defect-density homoepitaxial diamond films for electronic evaluation. To begin to examine this issue, X-ray topographs have been taken of natural and synthetic diamond single crystals. X-ray topography has revealed differences in the internal structure of type Ia [7] and type IIa diamonds (Figure 3). Although the type Ia diamond appears to show planar defects in projection, there appear to be fewer defects and defects with a lower degree of strain and/or crystallographic misorientation than the type IIa crystals. This is qualitatively consistent with the observations that type Ia diamond crystals tend to exhibit superior axial ion channeling characteristics than type IIa crystals [8]. While these results appear to indicate a trend, variations between different natural diamond crystals may not permit these results to be generally applicable to all diamond substrates of a given type. Also shown is an X-ray topograph of a synthetically produced type Ib diamond which has defects that appear to have propagated radially from the center of the crystal.

Substrate Cleaning

Both of the chemical cleaning procedures described above have been used, and both techniques have met with successful homoepitaxial growth. Unfortunately, the success has not been uniform and unequivocal. The reason for this has been that residual particulates remain on the surface of the diamond substrate. The effect of particulates on the surface is the nucleation of sporadic regions of polycrystalline diamond material interspersed throughout the homoepitaxial film. The particulates are believed to result from the commercial polishing processes, and apparently are not removed with wet chemical cleaning. Mechanically cleaning the substrates by swabbing with cotton-tipped swabs in deionized water will remove most of the particulates. This effect is shown dramatically in Figure 4 where a diamond substrate, which had been intentionally contaminated with particulates and then chemically cleaned (particulates still remain adherent), is shown to be free of these particulates after a short time ($\sim$ 1 min.) of swabbing.

Diamond Homoepitaxy

Figure 5 shows the change in surface morphology after 1 μm of diamond deposition on a diamond substrate. Before deposition the surface shows pits

and polishing scratches present. After deposition, the surface finish is greatly improved as little surface topography is visible. This planarization is an important feature for development of electronic devices in diamond.

The effect of surface planarization during homoepitaxial growth can also be illustrated using selective homoepitaxial deposition. Epitaxial lateral overgrowth (ELO) has been demonstrated using this low pressure rf-driven PECVD technique [9]. A lithographically patterned 200 nm thick Si mask, which substantially inhibits diamond nucleation, has been used to define the diamond "seeds" for homoepitaxial diamond growth. The overgrowth was best revealed by chemically etching the Si from the diamond. Figure 6 shows SEM of a cleaved cross-section showing diamond ELO. The sample has been sputter-coated with 10 nm of Pt to prevent charging during SEM examination. Growth of homoepitaxial diamond was observed to be approximately isotropic, extending over the Si mask by 0.45 μm and above the mask by 0.50 μm. There is evidence for smooth epitaxial growth above the diamond seed windows and faceting on the overgrowth. Comparing the surface of the epitaxial layer to the surface of the substrate, the initial substrate topography has been planarized by this diamond homoepitaxial deposition process.

Both macro- and micro-Raman spectroscopy have been routinely employed to assess the crystalline quality of the homoepitaxial diamond films. Spectra were excited using the 514.5 nm line of an Ar^+ ion laser with a micro-Raman spot size at the sample surface of < 5 μm. Shown in Figure 7 are micro-Raman spectra showing the 1332 cm^{-1} diamond LO phonon line taken from the selective-area homoepitaxial film and taken off the film where scattered and isolated polycrystalline diamond crystals have grown on the Si mask. The full-width at half-maximum (FWHM) values from these spectra differ by 1.6 cm^{-1} - with the homoepitaxial film having the narrower peak. This is consistent with the fact that the Raman signal from polycrystalline diamond films have greater FWHM than from single crystal diamonds. Another homoepitaxial diamond film with uniform coverage that was grown on a (100) type IIa substrate was examined with micro-Raman spectroscopy by focusing on the surface of the homoepitaxial film. The corresponding 1332 cm^{-1} diamond LO phonon line was found to have a FWHM of 2.1 cm^{-1}. Because of the small depth of focus of the micro-Raman system, it was also possible to focus into the bulk of the type IIa substrate. In this case, the FWHM increased to 2.4 cm^{-1}. Although this technique cannot completely isolate the Raman signals from the epitaxial film and the substrate, it shows qualitatively that this homoepitaxial diamond film is of greater perfection than the substrate. This same trend has been seen for homoepitaxial diamond grown on (100) type Ia diamond substrates, but the differential between the FWHM of the epitaxial film and the type Ia substrate is less (on the order of 0.1 cm^{-1}).

Summary

From the point of view of commercial availability, type Ia diamond substrates currently appear to be microstructurally superior for homoepitaxial growth. Although there remains diamond substrate surface topography concerns, if the substrates are mechanically and chemically cleaned properly and an adequate diamond deposition technique is used, the surface can be planarized for device fabrication. The evidence accumulated thus far indicates that homoepitaxial diamond films grown with rf PECVD are superior to the starting substrates. The ability to grow homoepitaxial diamond selectively with ELO allows for the possibility of creating films that are less microstructurally defective than the starting substrate.

Acknowledgements: The authors gratefully acknowledge the support of this work by the SDIO/IST through ONR, Contract No. N00014-86-C-0460. TPH and RJN gratefully acknowledge the support of this work by SDIO/IST through ONR, Contract No. N00014-90-J-1707.

REFERENCES

1. G.G. Fountain, R.A. Rudder, D.P. Malta, S.V. Hattangady, R.G. Alley, G.C. Hudson, J.B. Posthill, R.J. Markunas, T.P. Humphreys, R.J. Nemanich, V. Venkatesan, and K. Das, this proceedings.
2. Andrew R. Lang, 2nd Intl. Conf. on the New Diamond Science and Technology, Washington, DC, September 23-27, 1990, in press.
3. B.K. Tanner, *X-ray Diffraction Topography*. Pergamon Press, Oxford (1976).
4. W. Kern and D.A. Puotinen, RCA Rev., 31, 187 (1970).
5. R.A. Rudder, G.C. Hudson, Y.M. LeGrice, M.J. Mantini, J.B. Posthill, R.J. Nemanich, and R.J. Markunas, Mater. Res. Soc. Symp. Proc., EA-19, 89 (1989).
6. D.P. Malta, S.A. Willard, R.A. Rudder, G.C. Hudson. J.B. Posthill, R.E. Thomas, and R.J. Markunas, Proc. 49th Annual Meeting of the Electron Microscopy Society of America, (1991) in press.
7. The type Ia crystal examined in this study had a thin $\sim 0.5\mu$m epitaxial film grown selectively on it. The film was not visible, and its presence did not affect the X-ray topography images of the substrate microstructure.
8. G.S Sandu, N.R. Parikh, and M.L. Swanson, private communication of unpublished results, University of North Carolina, Chapel Hill, 1989.
9. R.A. Rudder, J.B. Posthill, G.C. Hudson, D.P. Malta, R.E. Thomas, R.J. Markunas, T.P. Humphreys, and R.J. Nemanich, 2nd Intl. Conf. on the New Diamond Science and Technology, Washington, DC, September 23-27, 1990, in press.

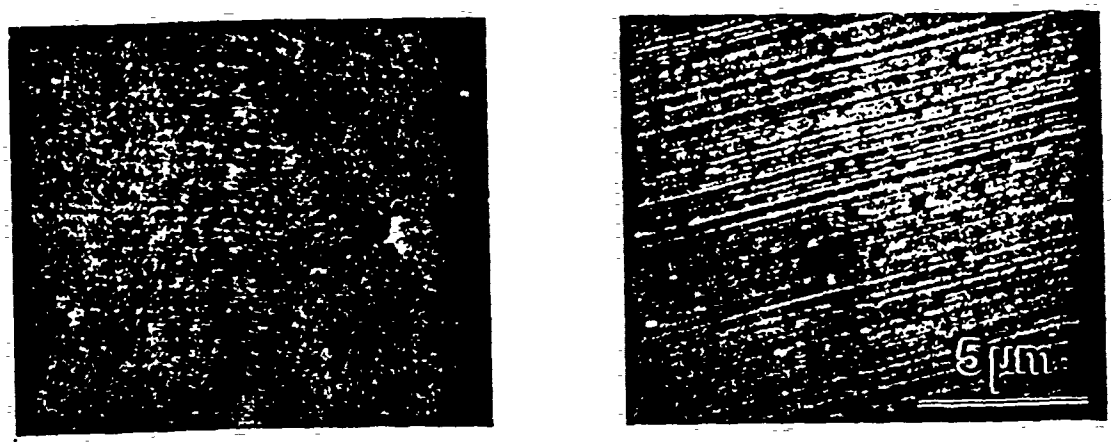

Figure 1. Surfaces of different as-received (100) type IIa diamond substrates.

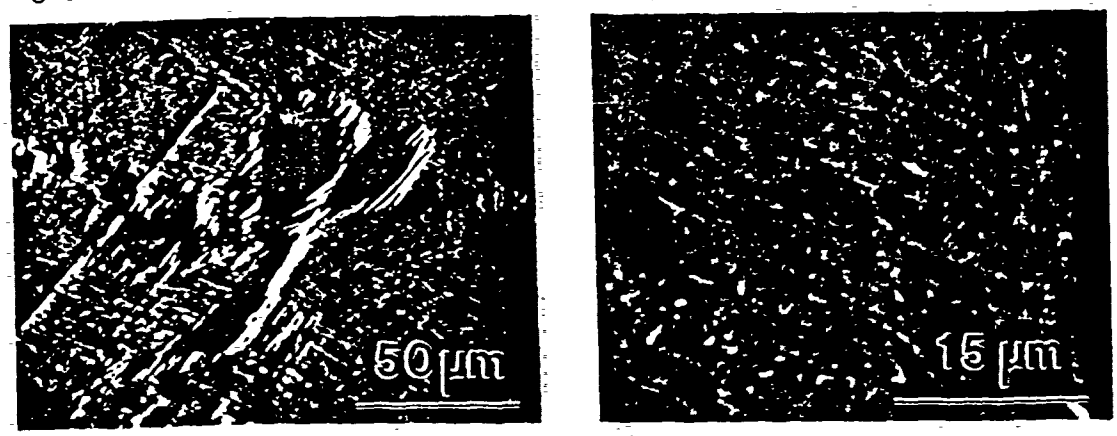

Figure 2. Surface of representative as-received (100) type Ib diamond substrate.

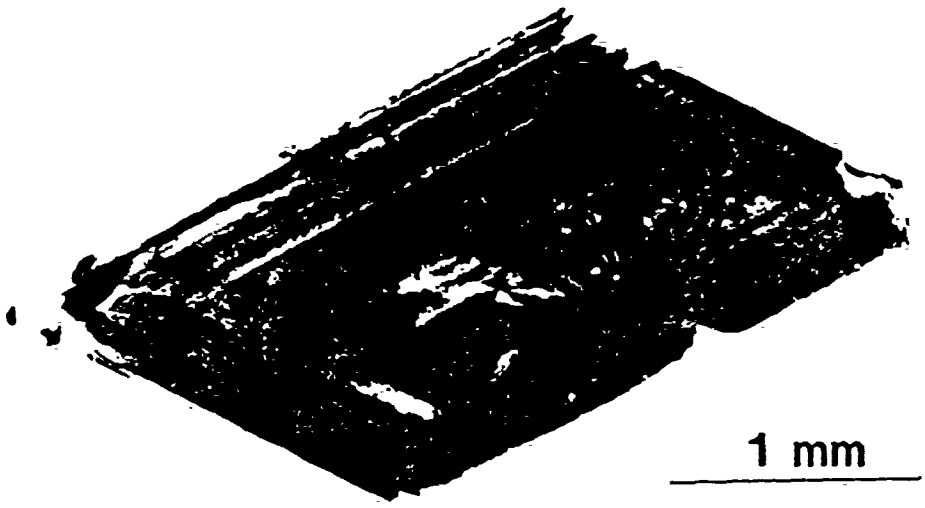

Figure 3. Representative X-ray topographs from: (A) type Ia diamond, $(0\bar{1}0)_{ST}$ [the radial defects are believed to have been created when the diamond was cleaved prior to analysis];

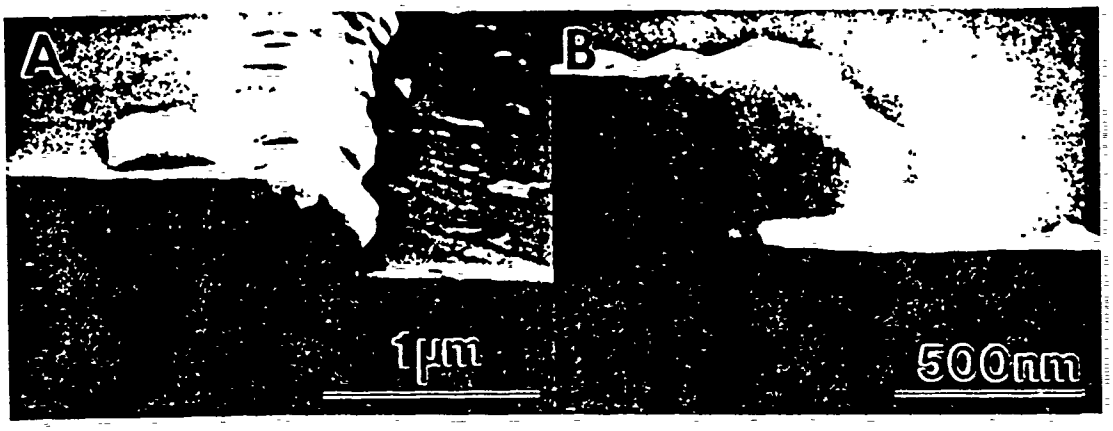

Figure 6. Cleaved cross-section showing ELO of diamond over a Si mask that has been chemically removed: (A) inclined view and (B) edge-on view.

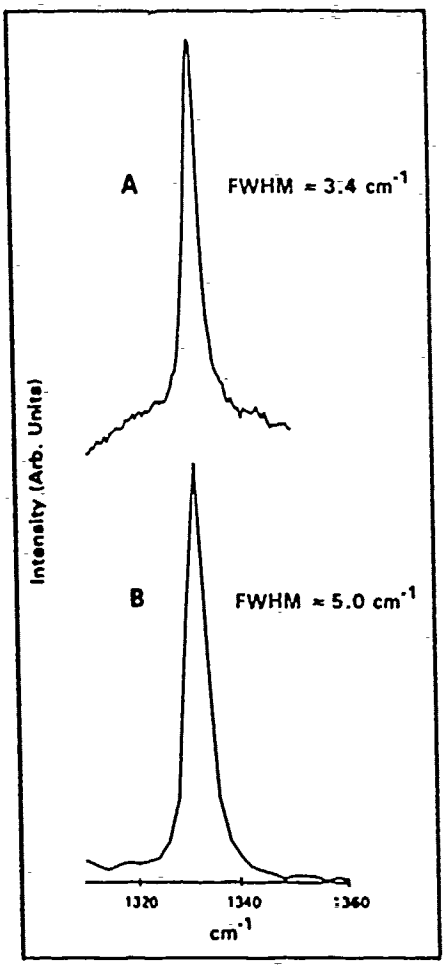

Figure 7. Micro-Raman spectra from: (A) selective-area homoepitaxial diamond (shown in Figure 6) and (B) polycrystalline diamond nucleated on mask (not shown in Figure 6 because it was etched off).

To be presented at the
179th Meeting of the Electrochemical Society
Washington, D. C. May 5 - 10, 1991

EFFECT OF THIN INTERFACIAL SiO_2 FILMS ON METAL CONTACTS TO BORON DOPED DIAMOND FILMS

V.VENKATESAN, K. DAS, D. L. DREIFUS

KOBE STEEL RESEARCH LABORATORIES, USA
ELECTRONIC MATERIALS CENTER
P. O. BOX 13608, RESEARCH TRIANGLE PARK, NC 27709

G. G. FOUNTAIN, R. A. RUDDER, J. B. POSTHILL, and
R. J. MARKUNAS

RESEARCH TRIANGLE INSTITUTE, RESEARCH TRIANGLE PARK, NC 27709-2194

ABSTRACT

The effect of thin interfacial films of SiO_2 (~20 Å) on the electrical characteristics of metal contacts fabricated on polycrystalline and homoepitaxial diamond films has been studied. These films were grown using plasma-enhanced chemical vapor deposition techniques. In order to minimize the effect of defects and / or hydrogen on the metal contact characteristics, these films were annealed at 950°C for 30 min. Metal-semiconductor contacts were formed by electron-beam evaporation of aluminum on both as-received and annealed polycrystalline films, whereas, gold metallization was used for the homoepitaxial film. Active diode dots were defined by a standard photolithographic process. It has been demonstrated that the introduction of a thin SiO_2 film at the interface between the metal and the diamond semiconductor film allows the fabrication of a rectifying contact, that is not otherwise possible for the films studied here.

INTRODUCTION

Semiconducting diamond, as a potential material for high temperature, high speed and high power device applications, has been the subject of some excellent reviews (1, 2). A number of these devices will rely on a rectifying metal / semiconductor contact for their operation. A metal / semiconductor contact also provides a suitable vehicle for electrical characterization of the device material. However, it has been observed that the formation of good rectifying contacts is not always easily accomplished on diamond films grown by chemical vapor deposition (CVD) (3). Contacts established with Al or Au on CVD films exhibit highly resistive ohmic or nominally asymmetric behavior, whereas these metals can be used almost routinely to form rectifying contacts on synthetic (4) and natural semiconducting diamond crystals (5). In the case of CVD grown homoepitaxial films, a chemical treatment in hot $CrO_3 + H_2SO_4$ solution has enabled the fabrication of Au

rectifying contacts (6). Characteristics of rectifying contacts on CVD grown films of both homoepitaxial (7) and polycrystalline diamond (8) have been improved by growing an insulating undoped diamond film on a previously deposited B doped semiconducting film.

In the present investigation, the effect of thin interfacial SiO_2 films on the electrical characteristics of metal contacts fabricated on B doped polycrystalline and homoepitaxial films has been studied. It has been demonstrated that the introduction of a thin SiO_2 film at the interface between the metal and the diamond semiconductor film allows the fabrication of a rectifying contact, that is not otherwise possible for the films studied here.

EXPERIMENTAL DETAILS

Both the polycrystalline and homoepitaxial B doped diamond films used for the study were grown using plasma-enhanced chemical vapor deposition (PECVD) techniques. The diamond films were materially characterized by scanning electron microscopy (SEM) and by Raman Spectroscopy. In addition, secondary ion mass spectroscopy (SIMS) analysis of selected samples were performed in order to determine the atomic concentration of B in the films.

As-deposited diamond films

A microwave plasma CVD reactor described in reference (9), was employed in this study for the deposition of the polycrystalline diamond films. These films were grown on low resistivity (<1 Ω cm) boron doped Si ((111) oriented) substrates using H_2 (99.5 %) and CH_4 (0.5 %) at a pressure of 35 torr. The substrates were maintained at 800°C during deposition. Moreover, these films were doped with boron using B_2H_6. Ratios of B_2H_6 to the total gas flow, of 0.002, 0.005, 0.008, 0.01, 0.05, 0.5 and 1.0 ppm were used to obtain films with a varied B concentration. In some cases O_2 (0.1 %) was also included in the gas mixture (for B_2H_6 ratios of 0.002, 0.005, 0.008 and 0.01 ppm). These films were grown for 14 hr. For the higher B_2H_6 ratios (0.05, 0.5 and 0.1 ppm) O_2 was not used and films were grown for 7 hr.

Details of the rf plasma CVD reactor utilized for the homoepitaxial film growth are given in reference (10). The homoepitaxial film was grown on a type I A insulating natural diamond crystal using 0.4 % CH_4 and 1 % CO in H_2 rf plasma. The film was also doped with B_2H_6 during growth.

Metal contacts on control samples without an SiO_2 interfacial layer were fabricated in the following way. After deposition the diamond films were cleaned using the RCA cleaning procedure (11). Approximately 2000 Å of aluminum was then electron-beam evaporated directly onto 0.002 ppm (B_2H_6 ratio) polycrystalline diamond sample to form a metal-semiconductor contact. For the homoepitaxial diamond sample a chemical treatment in hot $CrO_3 + H_2SO_4$ solution (to remove any non-sp^3 component in the diamond film) was also included and a gold metallization employed. An important point to note in the gold metallization procedure is that the electron-beam evaporation was a two step process. The deposition rate was 1Å/s for the first 100 Å of gold and then 5 Å/s for the rest of the ~ 2000Å film. This procedure markedly improved the adhesion of gold. Active diode areas, 100 μm in diameter separated from the field region by a 100 μm annular ring, were delineated by photolithography followed by Au or Al etching as the case may be. For the

photolithography process a mask pattern proposed by Ioannou et al.(12) was used. The 'infinitely' large area of the field-region ensured an adequate quasi-ohmic contact with the required current handling capability, particularly in the case of the homoepitaxial film that was deposited on an insulating natural diamond crystal.

Similar metal contact diodes were also fabricated on a 0.002 ppm (B_2H_6 ratio) polycrystalline diamond sample, which was deposited at the same time as the control sample. On this test sample ~ 20 Å thick film of SiO_2 was deposited by a remote plasma-enhanced CVD technique (13). Subsequently, this test sample was metallized with ~ 2000 Å Al. Active diode areas similar to those on the control sample were delineated by photolithography followed by Al etching. For the homoepitaxial film, following electrical measurements on the Au contacts fabricated on the control sample (i.e. without the SiO_2 interfacial film), the metal was etched in aqua regia (3HCl and $1HNO_3$). This test sample was then cleaned employing the RCA cleaning procedure and a ~ 20 Å thick film of SiO_2 was deposited. Approximately 2000 Å Au was subsequently electron-beam evaporated onto the test sample. Active diode areas were defined by photolithography and Au etching. Cross-sectional diagrams of the contact structure on the diamond films, (a) without, and (b) with the the SiO_2 film are shown in Fig. 1. The control and test samples were then electrically characterized using a HP 4145 B semiconductor parameter analyzer equipped with a probe station for high temperature measurements.

Heat treated diamond films

The polycrystalline films were annealed at a temperature of 950°C for 30 min, in order to minimize the effect of defects and/or hydrogen on the electrical characteristics of metal contacts on these films. Aluminum metal contacts were then fabricated on the annealed films both with and without an SiO_2 interfacial layer, following the procedure described in the previous section. Current-Voltage (I-V) measurements were then performed on these metal-semiconductor contacts. For the contacts fabricated on annealed 0.05 ppm (B_2H_6 ratio) samples with an SiO_2 interfacial layer, I-V measurements were conducted from room-temperature upto ~ 250 °C, at increments of ~ 50 °C.

RESULTS AND DISCUSSION

As-deposited diamond films

Scanning electron microscopy of the B-doped diamond films investigated here showed clear (111) facets and five-fold multiply twinned particles. Scanning electron microscopy also indicated that the polycrystalline diamond films grown with O_2 (lower B_2H_6 ratio) had a quality superior to those grown without O_2 (higher B_2H_6 ratio). The crystal quality was investigated using laser Raman spectroscopy. The Raman peak position characteristic of diamond was located near 1333 cm^{-1}. A relatively small sp^2 peak at 1500 cm^{-1} was also observed in the Raman spectrum of the diamond films. A SIMS analysis of the as-deposited 0.05 ppm (B_2H_6 ratio) diamond film showed an atomic B concentration of ~ 1.0×10^{18} cm^{-3}.

Current-voltage characteristics of Al contacts to as-deposited polycrystalline sample (0.002 ppm diborane concentration) are shown in Figs. 2 (a) and (b). Directly deposited Al contacts (Fig. 2 (a)) on this sample without the interfacial SiO_2 film showed near-ohmic I-

V characteristics. The subsequent introduction of the SiO_2 film provided rectifying characteristics as shown in Fig. 2 (b). Directly deposited Au contacts on the as-deposited homoepitaxial film also exhibited near-ohmic I-V characteristics as shown in Fig. 3 (a). With the introduction of the thin SiO_2 film good rectification is obtained as shown in Fig. 3 (b). In the presence of the SiO_2 film, low leakage currents (< 1 nA at 5 V) in the reverse direction were observed in both the polycrystalline and the homoepitaxial film. A breakdown voltage of ~7 V was observed for both as-deposited polycrystalline and the homoepitaxial films.

Heat treated diamond films

Current-voltage characteristics on Al contacts fabricated on annealed films with the lower B_2H_6 ratios, showed a drastic reduction in current in both the forward and reverse directions. Since the magnitude of the current was approximately the same in all the films (0.002, 0.005, 0.008 and 0.01 ppm B_2H_6 ratio), a representative plot from the 0.01 ppm sample is shown in Fig. 4. This reduction in current conduction on annealing is in conformity with observations reported by Landstrass et al. (14, 15), Albin et al. (16) and Muto et al. (17). Hydrogen dissociation and/or defect annihilation could account for the increased resistivity in these annealed diamond films.

Directly deposited Al contacts on annealed, 0.05 ppm (B_2H_6 ratio) polycrystalline sample without the interfacial SiO_2 film exhibited I-V characteristic, as shown in Fig. 5 (a). The subsequent introduction of the SiO_2 film provided rectifying characteristics as shown in Fig. 5 (b). A breakdown voltage of ~ 6 V was observed for this film. A background doping concentration of ~ 5.3×10^{18} cm^{-3} in this film was obtained using an approximate 'universal' expression for the breakdown voltage given by (18):

$$V_B = 60(E_g/1.1)^{3/2}(N_B/10^{16})^{-3/4}$$

where, V_B is the breakdown voltage for a plane-parallel junction, E_g, the band-gap of the material, and N_B, the doping concentration. A band gap of 5.45 eV for diamond and the experimentally observed breakdown voltage of 6 V was used in the above calculation. Assuming that the active B concentration in this high B concentration film is not very different from the atomic B concentration (~1.0×10^{18} cm^{-3}) as determined from SIMS analysis, the calculated value of the background doping concentration seems to agree within an order of magnitude with the SIMS results. It should be noted that for high concentrations of B of the order of 10^{19} - 10^{20} cm^{-3} in diamond, a complete activation of the impurity has been reported (19). However, it has not been established whether a similar effect can be expected at a B concentration of 1.0×10^{18} cm^{-3}. It should also be pointed out that a plane-parallel junction approximation will provide an underestimation of the breakdown voltage as edge effects are expected to produce a significant lowering of the breakdown voltage for a given doping concentration. An estimation of doping concentration from the observed breakdown voltage of the structute used here, therefore, will provide an overestimation of the doping concentration. Moreover, since the dielectric strength of SiO_2 is 10^7 V/cm (Appendix I of reference (18)) the breakdown voltage of ~ 20 Å SiO_2 film is ~ 2 V. This indicates that the experimentally observed breakdown voltage of this film (~ 6 V) is likely to be the breakdown voltage of the diamond film and not that of the dielectric. The I-V characteristics of this annealed diamond film (0.05 ppm B_2H_6 ratio) with interfacial SiO_2 measured at temperatures ranging from room temperature (RT) to 248

°C in ~ 50 °C increments, are shown in Fig. 6. It is seen that as the temperature is increased the reverse leakage current increases and the reverse breakdown voltage decreases. Nevertheless, a fairly good rectification behavior can be observed upto ~ 100 °C.

Conclusions

It has been demonstrated that the introduction of a thin SiO_2 film at the interface between the metal and the diamond semiconductor film allows the fabrication of a rectifying contact, that is not otherwise possible for the films studied here. This improvement in characteristics is probably due to a modification in the barrier height and field distribution and/or to passivation of the surface. Further work in this area is in progress to fully understand the reason for such behavior.

Acknowledgements

The authors are grateful to Dr. K. Kobashi, ERL, Kobe Steel, Ltd. Kobe, Japan, for providing the polycrystalline diamond films used in this study and to C. P. Tully, Kobe EMC for his assistance in prepation of the manuscript. GGF, RAR, JBP, and RJM gratefully acknowledge support from SDIO/IST through ONR (Contract No. N00014-86-C-0460).

References

1. A.T. Collins, Semicond. Sci. Technol. 4, 605 (1989).
2. G.Sh. Gildenblat, S.A. Grot, A. Badzian, to be published, Proc. IEEE.
3. V. Venkatesan, and K. Das, unpublished work, (1990).
4. G.H. Glover, Solid St. Elect. 16, 973 (1973).
5. E.C. Lightowlers and A.T. Collins, J. Phys. D : Appl. Phys. 9, 73 (1976).
6. S.A. Grot, G.Sh. Gildenblat, C.W. Hatfield, C.R. Wronski, A.R. Badzian, T. Badzian, R. Messier, IEEE Electron Dev. Lett. 11, 100 (1990).
7. H. Shiomi, Y. Nishibayashi and N. Fujimuro, presented at the 2nd Intl. Conf. New Diamond Sc. Tech., Washington, D.C., Sept 23-27 (1990).
8. K. Miyata, D.L. Dreifus, K. Das, J.T. Glass and K. Kobashi, to be presented at the Electrochem. Soc. Meeting, Washington, D.C., May 6-10 (1991).
9. 14. K. Kobashi, K. Nishimura, Y. Kawate, and T. Horiuchi, Phys. Rev. B 38, 4067 (1988).
10. R.A. Rudder, G.C. Hudson, Y.M. LeGrice, M.J. Mantini, J.B. Posthill, R.J. Nemanich, and R.J. Markunas, Mat Res. Soc. EA-19, 89 (1989).
11. W. Kern, and D. A. Puotinen, RCA Rev. 31, 187 (1970).
12. D. E. Ioannou, N. A. Papanicolaou, and P. E. Nordquist, Jr., IEEE Trans Electron Devices, ED-34, 1694(1987).
13. G.G. Fountain, R.A. Rudder, S.V. Hattangady, R.J. Markunas, and P.S. Lindorme, J. Appl. Phys. 63 (9), 4744 (1988).
14. M.I. Landstrass and K.V. Ravi, Appl. Phys. Lett. 55, 975 (1989).
15. M.I. Landstrass and K.V. Ravi, Appl. Phys. Lett. 55, 1391 (1989).
16. S. Albin and L. Watkins, IEEE Electron Dev. Lett. 11, 159 (1990).
17. Y. Muto, T.Sugino, J. Shirafuji and K. Kobashi, submitted for publication: Appl. Phys. Lett. (1990).

18. S.M. Sze, 'Physics of Semiconduction Devices', Wiley-Interescience publication, New York, 1981.
19. K. Nishimura, K. Das and J.T. Glass, J. Appl. Phys. 69, 3142 (1991).

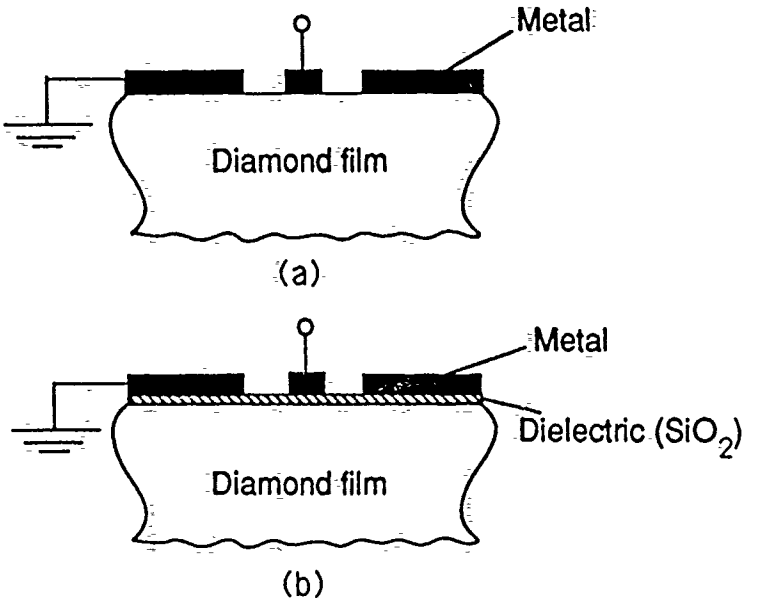

Figure 1: Cross-sectioal diagram of contact structure on diamond film, (a) without dielectric layer and (b) with dielectric layer.

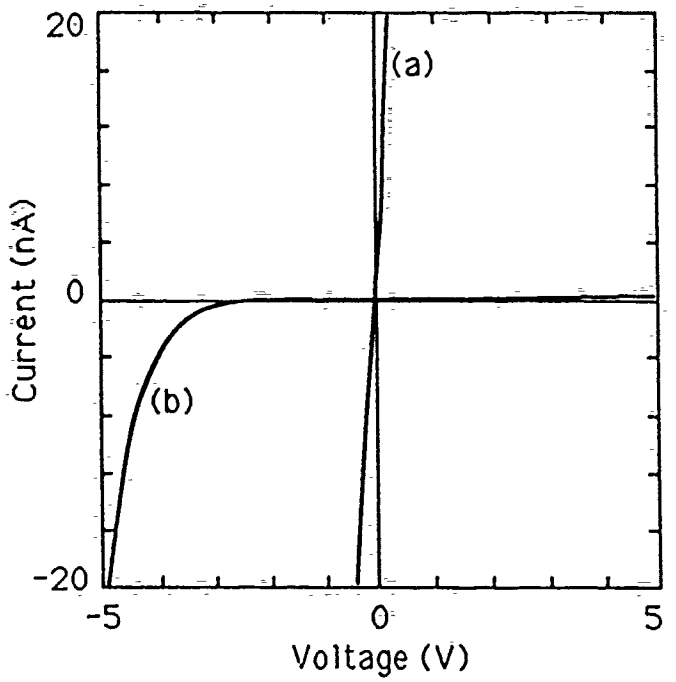

Figure 2: Current-voltage characteristics of Al contacts on polycrystalline diamond film (0.002 ppm), (a) direct metalization and (b) with interfacial SiO_2.

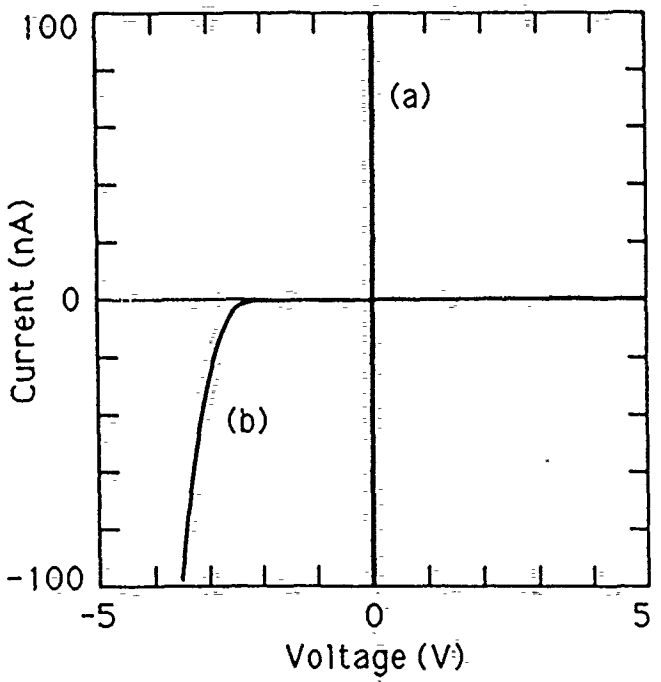

Figure 3: Current-voltage characteristics of Au contacts on homoepitaxial diamond film, (a) direct metalization and (b) with interfacial SiO_2 .

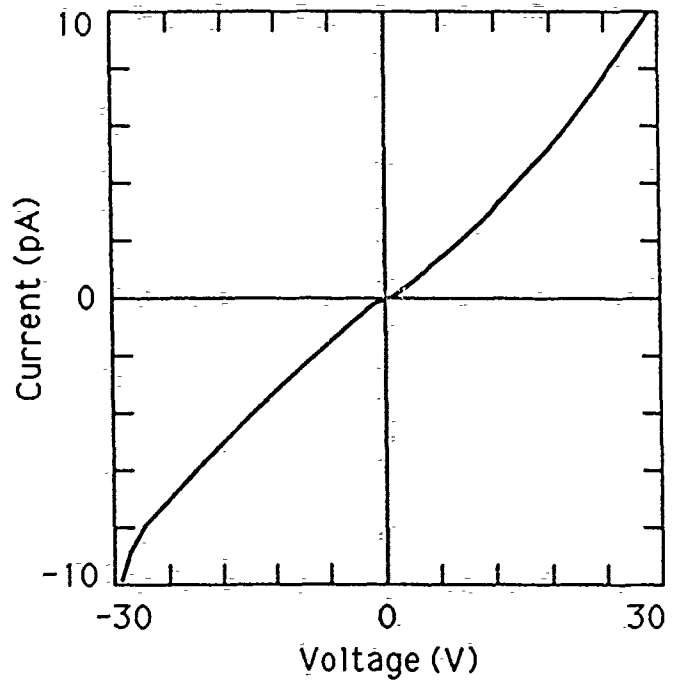

Figure 4: Current-voltage characteristic of Al contacts on annealed diamond film (0.01 ppm).

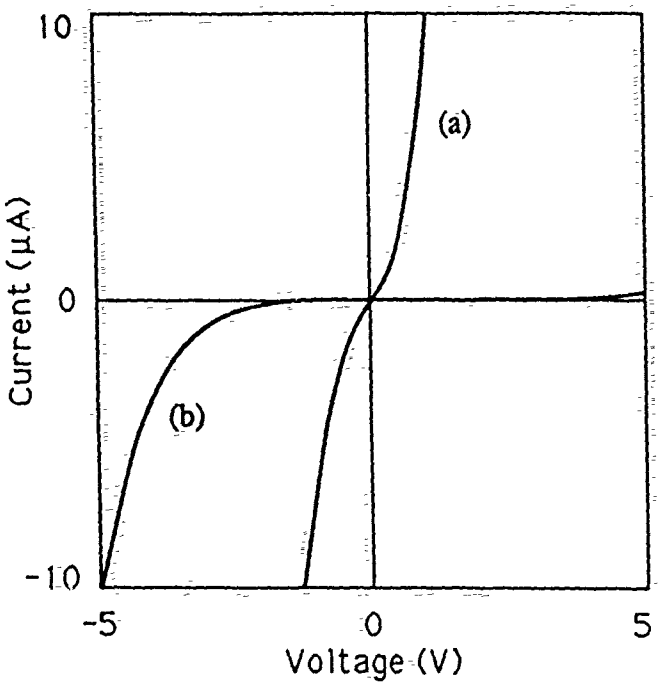

Figure 5: Current-voltage characteristic of Al contacts on annealed diamond film (0.05 ppm), (a) direct metalization and (b) with interfacial SiO_2.

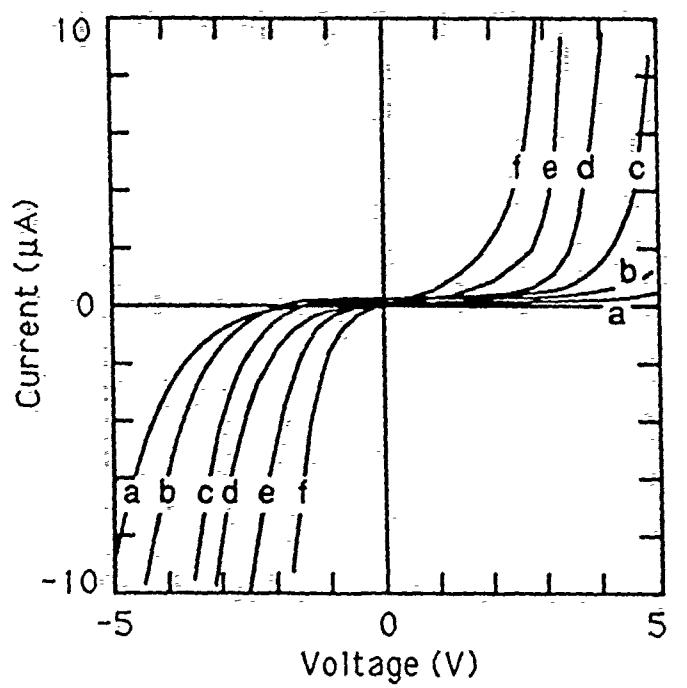

Figure 6: Current-voltage characteristic of Al contacts on annealed diamond film (0.05 ppm) with interfacial SiO_2 at (a) RT, (b) 50°C, (c) 99°C, (d) 149°C, (e) 198°C, and (f) 248°C.

IGFET FABRICATION ON HOMOEPITAXIAL DIAMOND USING IN SITU BORON AND LITHIUM DOPING

G.G. Fountain, R.A. Rudder, D.P. Malta, S.V. Hattangady,
R.G. Alley, G.C. Hudson, J.B. Posthill, and R.J. Markunas
Research Triangle Institute, Research Triangle Park, NC 27709

T.P. Humphreys and R.J. Nemanich
North Carolina State University
Raleigh, NC 27695-8202

V. Venkatesan and K. Das
Kobe Steel Research Laboratories
Electronic Materials Center
Research Triangle Park, NC 27709

ABSTRACT

The use of boron and lithium as dopant impurities in diamond has been investigated using diborane and lithium fluoride as in situ dopant sources. The lithium was investigated as a possible n-type dopant. The diamond material, grown by rf plasma discharge at low pressure, was characterized electrically and microstructurally. The boron was found to be p-type, as expected, with an activation energy of 0.24 eV. The lithium doped material was also found to be p-type with a similar activation energy. SIMS data indicates that the lithium doped samples also contain significant concentrations of boron, enough to account for the electrically active species. However the mobility of the carriers in the lithium/boron doped material seem to be somewhat higher. Schottky barrier diodes were formed on the lithium/boron doped material which showed good rectifying behavior. The minority carrier diffusion length in the material was estimated from EBIC measurements to be $\sim 0.5\ \mu m$. The lithium appears to be electrically inactive in this material, although it may improve the electrical characteristics of the material. IGFET devices were fabricated in the boron doped and lithium boron doped materials using a selective deposition fabrication scheme. The boron doped device exhibited a transconductance of 38 μS/mm.

Introduction

The extremely selective nature of the plasma activated diamond deposition processes provides a very useful and flexible vehicle for device fabrication sequences. Other workers have already reported diamond insulated gate field effect transistor (IGFET) fabrication using selective diamond deposition with a sputtered quartz insulator [1]. The doping of active layers for diamond devices is a crucial topic and is currently under study by several groups [2,3,4]. Boron has been established as a p-type

dopant for diamond. Boron doping has been accomplished using solid boron etched in situ and using diborane as a gaseous source. Although there have been specific reports of the formation of n-type diamond [5], this is still an area that requires further development. Li has been proposed as a potential n-type dopant for diamond based on theoretical modelling [6]. We have undertaken a preliminary study to investigate the suitability of using LiF as a solid source to dope diamond growing in a plasma-enhanced chemical vapor deposition (PECVD) environment. In this paper, we report fabrication of a diamond IGFET structure using selective diamond deposition with boron and lithium doping in conjunction with a remote plasma enhanced chemical vapor deposition (RPECVD) of a SiO_2 insulating dielectric layer.

Doping Studies

The system used for the growth of homoepitaxial diamond consists of a 13.56 MHz inductively-coupled PECVD system. A gas mixture of 98.5% H_2, 1.0% CO and 0.5% CH_4 flowed through a 62.5 mm quartz tube at a rate of 30 sccm at 5.0 Torr. The sample is positioned near the rf coil on a graphite susceptor and is held at $\sim 800\,^{\circ}C$ during growth. Type Ia and IIa natural (100) diamond crystals were used in these studies. Boron and lithium were investigated as in situ dopants.

Boron doping was accomplished by introducing diborane diluted in H_2 into the reactor during diamond deposition. The diborane source was diluted in hydrogen to 1000 ppm. The diborane was leaked into the chamber with a flow rate of less than 0.5 sccm. Calculations bases on the partial pressure of diborane indicate that the incorporation efficiency is on the order of unity.

Lithium doping was accomplished via introduction of a solid source of LiF on the graphite susceptor during the deposition, or via introduction of the solid source to "dose" the reactor prior to loading the substrate for diamond growth. It was found that under diamond growth conditions, the LiF is dissolved by the atomic hydrogen in the reactor. Lithium emissions were observed in the reactor once the sources began to volatilize. Diamond deposition, with a Li source present in the reactor, resulted in high incorporation of Li into the samples ($> 10^{20}\,cm^{-3}$). Consequently, growths were performed with no source of Li in the reactor other than the Li residing on the chamber fixtures following "reactor dosing". Typically, a solid source would be introduced into the reactor, a discharge initiated, whereby emissions of Li were detected, the solid source removed, and the reactor deconditioned by a hydrogen discharge to reduce the Li concentration in the reactor prior to epitaxial growth.

Electrical and Physical Analysis of Doped Diamond Films

The doped diamond samples were characterized by Van der Pauw Hall measurement for carrier density and mobility. The measurement was carried out as a function of temperature to attain activation energies of the dopant species.

The boron doped samples were determined to be p-type as expected with a carrier density in the $10^{17}cm^{-3}$ range. Two levels were seen in the plot of carrier density vs. temperature as shown in Figure 1. One had a low activation energy of 0.0062 eV, and the other had an activation energy of 0.24 eV. The origin of the low activation energy level is unknown at this point. The 0.24 eV level is more characteristic of boron activation in diamond [3]. Hall mobilities measured were on the order of 45 $cm^2/Vsec$. It is likely that the boron is compensated by some other level in the diamond, possibly a damage or crystalline defect related level.

Lithium samples were also characterized by Hall measurements. Data from a heavily lithium doped sample is shown in Figure 2. Data from a more lightly doped sample is shown in Figure 3. Both samples exhibit p-type behavior, which was unexpected. The activation energies of the acceptor levels in the samples seemed surprisingly close to the level measured for the boron doping. The lightly doped sample did however exhibit the higher mobility than the boron doped sample.

SIMS analysis of the heavily lithium-doped sample showed both Li and B in the film. The amount of Li was $\sim 10^{21} cm^{-3}$; the amount of B was $\sim 10^{18} cm^{-3}$. The source of the boron is at this point undetermined; however, it is likely to be a deposition system component. It is very probable that the p-type behavior is from the boron in the film and not the lithium. The lithium does, however, seem to have a beneficial effect on the electrical properties of the film.

Au Schottky diode structures were fabricated on a heavily lithium-doped sample that had received a 30 minute hydrogen plasma treatment (1500 watts of RF power into the plasma), at 5 Torr, at approximately 700 ° C. These diodes showed good rectification behavior with a turn-on voltage of 2.5 V and a breakdown voltage of 6 to 8 V. The reverse leakage current is on the order of 12.5 $\mu A/cm^2$. Au contacts which had been deposited on material doped with boron alone (which had received a similar hydrogen plasma treatment) exhibited ohmic behavior.

The Au Schottky contact was used to perform electron-beam induced current (EBIC) measurements. EBIC was used to estimate the minority-carrier diffusion lengths. A thin Au Schottky contact was used for charge collection, and the induced current was measured as a function of distance, in plan-view, from the contact. For primary beam energies from 10keV - 20 keV, the minority-carrier diffusion length was measured to be 0.5μm. This compares with measured minority-carrier diffusion lengths of $\sim 3\mu$m in natural type IIb diamond (B-doped) [7].

Diamond IGFET Fabrication and Testing

Transistor structures were fabricated on a Type IA natural diamond (100) substrate from Drucker-Harris. The diamond substrate was cleaned using a conventional RCA wet chemical clean [8]. Polysilicon layers as well as SiO_2-polysilicon composite

layers were used as masking materials. During diamond deposition the top layer of the silicon is carbonized making it impervious to the hydrogen etching environment. It was found that SiO_2 masks were removed by the hydrogen environment if no oxygen was used in the process. The composite structure assures that the carbonized silicon layer can be removed from the wafer. The mask was patterned using standard lithographic techniques and wet etching to open holes for deposition of the conducting p-type diamond areas. Following diamond deposition, the silicon mask was etch removed. The sample was then coated with a 250 Å RPECVD SiO_2 gate dielectric. This process has been used to deposit low temperature, gate-quality dielectrics on Si and other semiconductors [9,10]. Titanium gate electrodes were formed using liftoff. Source-drain contact openings were patterned and openings etched in the oxide using buffer HF solution. Titanium contacts were formed using liftoff. The contacts were ohmic as deposited. The gate length and width of the transistors was 8μm and 50μm, respectively.

Two types of working IGFET structures were fabricated, one using boron doping alone and one using the lithium doping. In both cases a major limitation on the device fabrication process was control of the dopant concentration.

The boron doped diamond IGFET source drain I-V characteristics are shown in Figure 4. The device showed transistor action characteristic of a p-channel, depletion mode device. The device cannot be pinched off with the available gate voltage. The leakage current is most likely due to defects in the material or surface leakage. The maximum transconductance of the device is 38 μS/mm at 8 V drain to source. The transconductance of the device is slightly larger for the 1 to 2 V gate step than for the 0 to 1 V gate step. This increase in transconductance with increasing depletion is indicative of a relatively high density of surface states at or near the diamond/SiO_2 interface. The geometry of the FET is such that the source to gate resistance is on the order of $2 \times 10^5\ \Omega$. This resistance would decrease the transconductance of the device by a factor of about 2.

The diamond material used for the transistor channel had a resistivity of 12 Ω-cm. The specific contact resistance of the titanium contacts on this material were measured using a transmission line model test structure. The specific contact resistance is 0.09 Ω-cm^2. Titanium contacts were also fabricated on heavily boron doped material with a resistivity of 0.08 Ω-cm. These contacts exhibited a specific contact resistance of $1.4 \times 10^{-4}\ \Omega$–cm^2. Such layers could be used for contact layers to reduce parasitic resistances in the source and drain using an additional selective diamond deposition step.

The lithium/boron doped diamond IGFET source drain I-V characteristics are shown in Figure 5. This device exhibited much better saturation behavior than the boron doped device. This device has a more lightly doped channel than the boron doped device as evidenced by the lower saturation current. This device showed both depletion and enhancement behavior. However it is not clear whether this enhanced current is due to accumulation of a conducting layer at the surface or just un-depleting

of the channel. It is likely that, since the doping level is approximately 2 orders of magnitude lower in this device than the first device, the channel is nearly fully depleted at 0.0 V gate bias. The device has a substantial leakage current. Comparison of this leakage current level with the leakage between isolated devices indicated that the current is principally substrate current.

Conclusions

In situ boron and lithium doping of diamond has been carried out using a diborane gas source and a lithium fluoride solid source in a low pressure rf diamond deposition process. The boron was found to be p-type with an activation energy of 0.24 eV. The lithium was judged to be electrically inactive in the material evaluated here. The activation energy of the conductivity along with SIMS data on impurity levels indicated that the conduction is probably due to unintentionally incorporated boron in the film. The lithium appeared to have some beneficial effects on the electrical properties of the the doped diamond films. This effect requires further study. Working IGFET devices were fabricated using the boron doped material and the lithium/unintentional boron doped material. A maximum transconductance of 38 μS/mm was measured for the boron doped device. Improvements in device performance could be achieved through reducing the source drain parasitic resistances and by improving the diamond/SiO_2 interfacial characteristics.

Acknowledgements The authors wish to thank the Strategic Defense Initative Organization/Innovative Science and Technology Office through the Office of Naval Research (N-00014-86-C-0460) for the financial support of this work. TPH and RJN gratefully acknowledge the support of this work by the ONR, Contract No. N00014-90-J-1707.

REFERENCES

1. S.A. Grot, C.W. Hatfield. G. Sh. Gildenblat, A.R. Badzian, and T. Badzian, presented at the Second International Conference on the New Diamond SCience and Technology (ICNDST-2), Washington, DC(USA), September 23-27, 1990.

2. Naoji Fujimori, Kideaki Nakahata, and Takahiro Imai, Jap. J. Appl. Phys. 29, 824 (1990).

3. B.V. Derjaguin, B.V. Spitsyn, A.E. Goridetsky, A.P. Fakharov, L.L. Bouilov, and A.E. Sleksenko, J. Cryst. Growth, 31, 44 (1975).

4. G.Sh. Gildenblat, S.A. Grot, C.W. Hatfield, C.R. Wronski, A.R. Budzian, T. Badzian, and R. Messien. Mat. Res. Soc. Symp. Proc. 162, 297 (1990).

5. Ken Okano, Hideo Kiyota, Tatsuya Iwasaki, Tateki Kurosu, Masamori Iida and Terutaro Nakamura, presented at ICNDST-2, Washington, DC(USA), September 23-27, 1990.

6. J. Bernholc, S. Kajihara, and A. Antonelli, presented at ICNDST-2, Washington, DC(USA), September 23-27, 1990.

7. D.P. Malta, S.A. Willard, J.B. Posthill, and R.J. Markunas, unpublished results, Research Triangle Institute, 1989.

8. R.A. Rudder, G.C. Hudson, Y.M. LeGrice, M.J. Mantini, J.B. Posthill, R.J. Nemanich, and R.J. Markunas, Mat. Res. Soc. EA-19, 89 (1989).

9. G.G. Fountain, R.A. Rudder, S.V. Hattangady, R.J. Markunas, P.S. Lindorm, J. Appl. Phys., 63, 4744 (1988).

10. D.J. Vitkavage, G.G. Fountain, R.A. Rudder, S.V. Hattangady, R.J. Markunas, Appl. Phys. Lett., 53, 692 (1988).

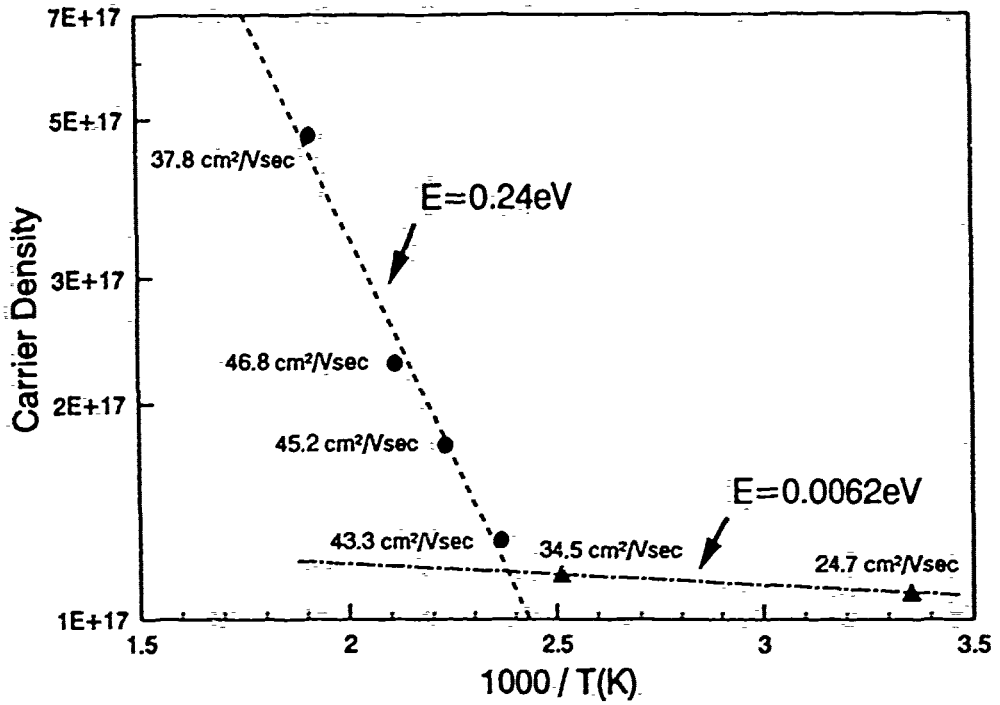

Figure 1 Carrier concentration vs. reciprocal temperature for a boron-doped homoepitaxial film. The material is p-type. Hall mobilities are listed.

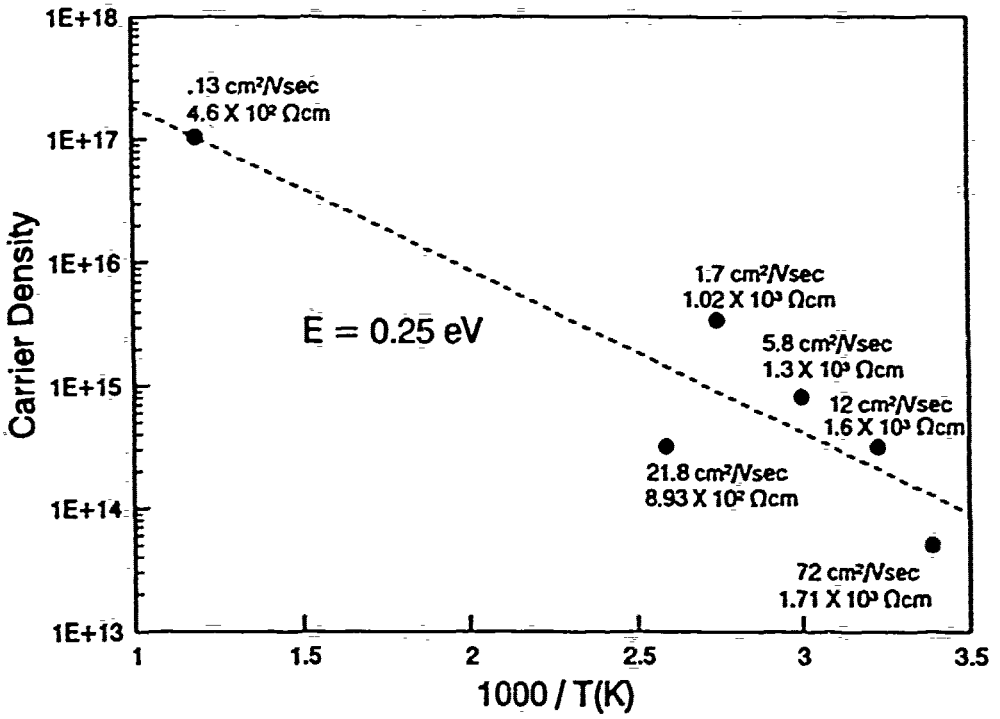

Figure 2 Carrier concentration vs. reciprocal temperature for a heavily Li doped homoepitaxial film. The material is p-type, probably due to boron contamination. Hall mobilities are listed.

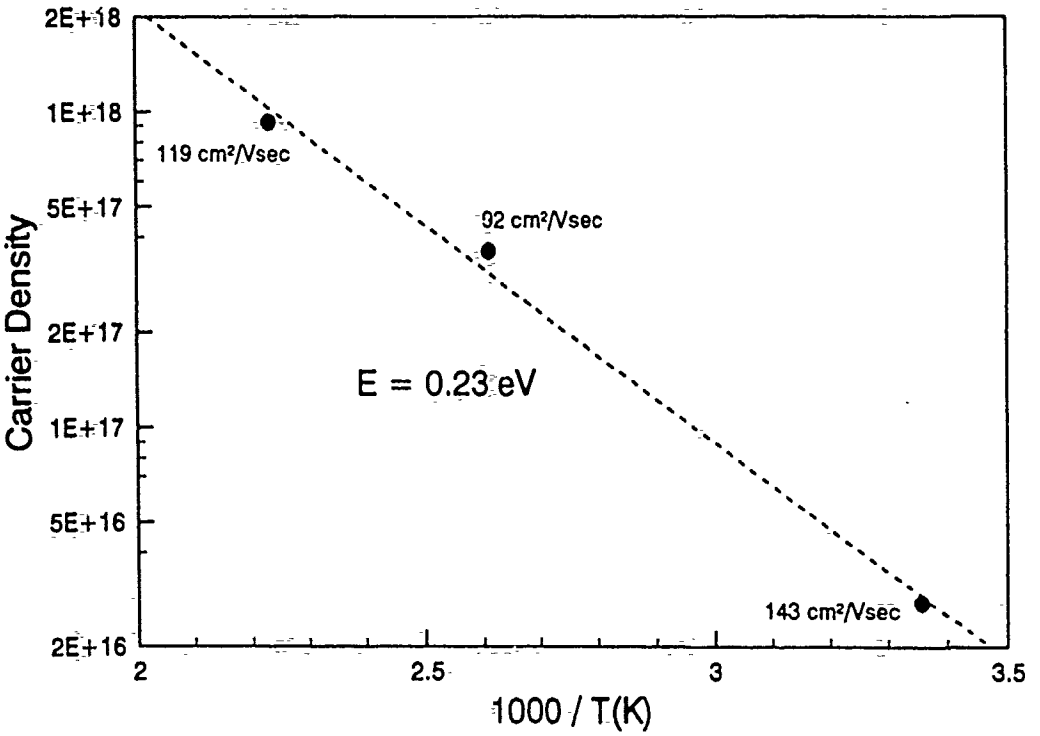

Figure 3 Carrier concentration vs. reciprocal temperature for a lightly Li doped homoepitaxial film. Note the improved Hall mobilities.

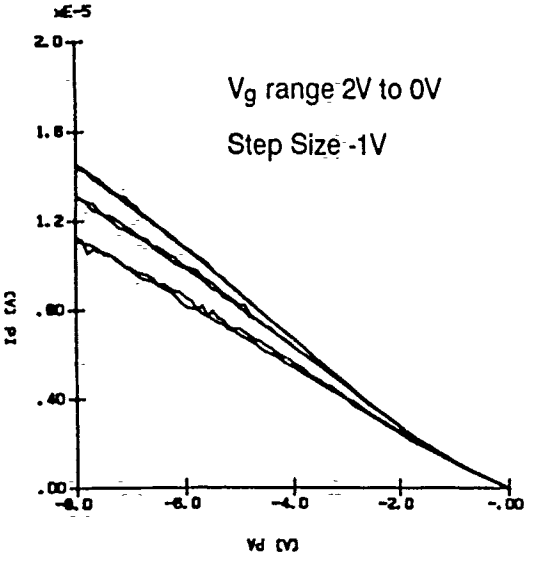

Figure 4 Drain Source I-V characteristic from Boron doped IGFET.

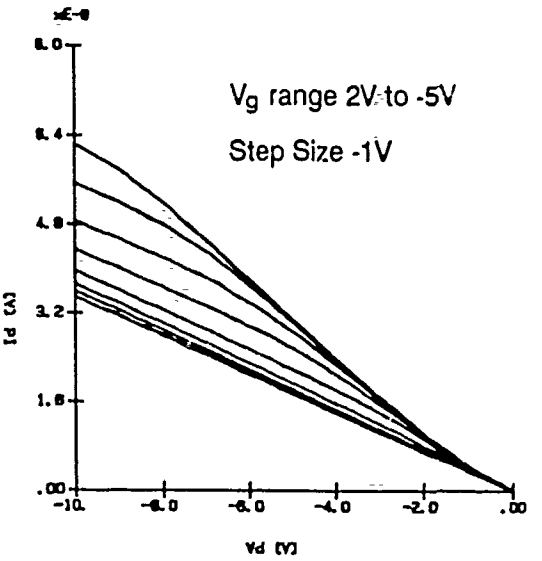

Figure 5 Drain Source I-V characteristic from Lithium/Boron doped IGFET